

One-dimensional model of chiral fermions with Feshbach resonant interactions

Abhinav Prem^{1,*} and Victor Gurarie¹

¹*Department of Physics and Center for Theory of Quantum Matter,
University of Colorado, Boulder, Colorado 80309, USA*

We study a model of two species of one-dimensional linearly dispersing fermions interacting via an s-wave Feshbach resonance at zero temperature. While this model is known to be integrable, it possesses novel features that have not previously been investigated. Here, we present an exact solution based on the coordinate Bethe Ansatz. In the limit of infinite resonance strength, which we term the strongly interacting limit, the two species of fermions behave as free Fermi gases. In the limit of infinitely weak resonance, or the weakly interacting limit, the gases can be in different phases depending on the detuning, the relative velocities of the particles, and the particle densities. When the molecule moves faster or slower than both species of atoms, the atomic velocities get renormalized and the atoms may even become non-chiral. On the other hand, when the molecular velocity is between that of the atoms, the system may behave like a weakly interacting Lieb-Liniger gas.

I. INTRODUCTION

Recent advances in the cooling and trapping of ultracold atomic gases, coupled with the ability to tune interactions via Feshbach resonances [1–5], have made accessible the regime of strong correlations in many body physics. In particular, it has become possible to confine quantum gases to effectively one-dimensional (1D) geometries, where the effects of strong correlations are enhanced. The experimental realization of strongly interacting 1D systems, such as the Tonks-Girardeau gas [6, 7], the super-Tonks-Girardeau gas [8], and Fermi gases close to a Feshbach resonance [9–11], thus provides exciting new opportunities for studying the many-body physics of 1D quantum gases. Recently, considerable theoretical attention has also been paid to 1D Bose-Fermi mixtures, since these are realizable through current cold atom experiments [12–20].

One such experimentally relevant system is that of a 1D spin-1/2 gas of fermions, where it is now routine to tune the atoms forming the gas close to a Feshbach resonance, which induces controllable interactions amongst the fermionic atoms. This system of fermionic atoms, confined to a 1D geometry and interacting via an s-wave Feshbach resonance, can be described by the following Hamiltonian,

$$H_F = \int dx \left[\sum_{\sigma=\uparrow,\downarrow} \hat{a}_\sigma^\dagger \left(-\frac{\partial_x^2}{2m_a} \right) \hat{a}_\sigma + \hat{b}^\dagger \left(-\frac{\partial_x^2}{2m_b} \right) \hat{b} + \epsilon_0 \hat{b}^\dagger \hat{b} + g(\hat{b}^\dagger \hat{a}_\uparrow \hat{a}_\downarrow + h.c.) \right], \quad (1)$$

where \hat{a}_σ^\dagger , \hat{a}_σ are fermionic creation and annihilation operators for the open-channel atoms (here σ refers to two hyperfine states of these atoms, labelled by \uparrow and \downarrow),

\hat{b}^\dagger , \hat{b} are those for the closed-channel bosonic molecules formed by the atoms, m_a and m_b are their respective masses, ϵ_0 is the bare detuning—which can be changed in an experiment by varying the magnetic field applied to the atoms—and g is the atom-molecule interconversion strength. This model, which first appeared in the context of high temperature superconductivity (in three spatial dimensions) [21], is usually referred to as “the boson-fermion resonance” or “two-channel” model, and describes the BCS-BEC crossover in fermionic paired superfluids [22–25].

In actual experiments, the parameter g is usually very large, a situation which is typically referred to as the broad resonance regime. Under the assumptions of a large interconversion strength g , it is possible to integrate out the molecules to arrive at a purely fermionic Hamiltonian,

$$\hat{H} = \int dx \left[\sum_{\sigma=\uparrow,\downarrow} \hat{a}_\sigma^\dagger \left(-\frac{\partial_x^2}{2m_a} \right) \hat{a}_\sigma - \frac{g^2}{\epsilon_0} \hat{a}_\downarrow^\dagger \hat{a}_\uparrow^\dagger \hat{a}_\uparrow \hat{a}_\downarrow \right]. \quad (2)$$

This is the familiar and well studied model of two species of fermions interacting via a short range interaction, where the strength of this interaction can be controlled by tuning the parameter ϵ_0 .

An attractive feature of the resulting one-channel model Eq. (2) is that it is exactly solvable by the Bethe Ansatz technique [26]. First found independently by M. Gaudin [27, 28] and by C.N. Yang [29] in 1967 as an abstract exercise, the exact solution for this model is now widely used to describe the experiments on 1D fermionic gases interacting via a Feshbach resonance [30, 31].

However, it is in principle possible to conduct experiments in the case where g is not large, usually termed the narrow resonance regime. In this regime, the physics of these 1D Bose-Fermi mixtures is described by the full model Eq. (1) and can well be richer than that of the short ranged interacting fermions described by Eq. (2).

Unfortunately, the model given by Eq. (1) is not integrable and cannot be solved exactly [32]. This model is

* abhinav.prem@colorado.edu

however amenable to analysis via the bosonization technique, a program which was carried out in Refs. [33, 34]. This analysis indeed uncovers additional phases which fermions confined to a 1D geometry and interacting via a narrow Feshbach resonance can form, as compared to the simpler case of a broad resonance.

However, bosonization is an approximate technique and its application to any particular problem requires making certain assumptions about the possible phases one expects the system to form. It is therefore of considerable interest to have a model of Feshbach resonance which would be exactly integrable in 1D space and thus be exactly solvable, without having to rely on any assumptions.

Such an integrable, and thus exactly solvable, model of narrow Feshbach resonance in 1D space indeed exists in the literature. Called the Quantum Three Wave Interaction (Q3WI) model, it differs from Eq. (1) in that the particles it describes are chiral and move just in one direction. Its Hamiltonian is given by

$$\hat{H} = \int dx \left[\sum_{\sigma=1,2} \hat{a}_{\sigma}^{\dagger} (-iv_{\sigma} \partial_x) \hat{a}_{\sigma} + \hat{b}^{\dagger} (-iu \partial_x) \hat{b} + \nu \hat{b}^{\dagger}(x) \hat{b}(x) + g \left(\hat{b} \hat{a}_1^{\dagger} \hat{a}_2^{\dagger} + h.c. \right) \right], \quad (3)$$

where the $\hat{a}_{1,2}$ are fermionic annihilation operators for atoms and \hat{b} is that for the bosonic molecules, v_1 and v_2 are the velocities of the chiral fermions, while u is that of the molecule. ν is the detuning and g the interconversion strength; both are parameters that control the strength of the resonance. Note that the single particle spectrum of Eq. (3) is unbounded from below. However, as is usual, in our study we will assume a certain cut-off for the allowed values of particle momenta. In its presence, Eq. (3) has a well defined ground state.

This model was shown to be integrable in Refs. [35, 36] and while the thermodynamic behavior was studied in Ref. [37], the authors of that work did not uncover the different regimes that appear in this model.

Here, we exploit the exact solubility of the Q3WI model through the Bethe Ansatz and study in detail its behavior in the thermodynamic limit. In particular, we analytically study the strongly ($g \rightarrow \infty$) and weakly ($g \rightarrow 0$) interacting limits of this model at zero temperature. Interestingly, we find that in the latter limit this system can undergo various phase transitions and, depending on the model parameters, can form unconventional phases such as one where the system remains non-interacting deep within the Fermi sea or one where the density of fermions diverges in the limit where the coupling g goes to zero, similarly to the weakly interacting Lieb-Liniger gas.

Before summarizing our main results, we first address the feasibility of realizing such a chiral model. The Q3WI model Eq. (3) can be obtained from more realistic non-chiral models similar to Eq. (1) if the fermion momenta

are restricted to lie in the vicinity of certain Fermi points. One simple way to generate this model is to either consider fermionic atoms in a single hyperfine state or to consider spin-polarized fermions. Suppose that all atomic states with their momenta restricted to lie in the interval $k_{f1} < k < k_{f2}$ are filled. Further, suppose that this gas is close to a p -wave Feshbach resonance, which can turn pairs of fermions into bosons. Such a system is described by the atom-molecule interconversion term

$$H_p = \int dx \left[\hat{a}^{\dagger} \left(-\frac{\partial_x^2}{2m_a} \right) \hat{a} + \hat{b}^{\dagger} \left(-\frac{\partial_x^2}{2m_b} \right) \hat{b} + g_p \int dx \left(\hat{b} \left(\hat{a}^{\dagger} \partial_x \hat{a}^{\dagger} - \partial_x \hat{a}^{\dagger} \hat{a}^{\dagger} \right) + h.c. \right) \right]. \quad (4)$$

Expanding the operator \hat{a}^{\dagger} in Fourier series and concentrating on the vicinity of momenta k_{f1} and k_{f2} , we reproduce the interaction term in Eq. (3), with indices 1 and 2 referring to the modes of \hat{a}^{\dagger} in the vicinity of the momenta k_{f1} and k_{f2} respectively. Note that ‘forward scattering,’ the terms where all momenta are restricted to the vicinity of one of the two points k_{f1} or k_{f2} , will be suppressed when the momentum transferred to \hat{b} is small (that is, they will be proportional to the momentum transfer).

The kinetic energy in Eq. (3) is then obtained by linearising the momenta in the vicinity of the Fermi points k_{f1} and k_{f2} , as well as linearising the molecular momenta in the vicinity of $k_{f1} + k_{f2}$. In the continuum, we have that $m_b = 2m_a$, in which case the molecular velocity is fixed by that of the atoms, $u = (v_1 + v_2)/2$. While our solution for the Q3WI captures this regime (see Sec. VII), this setting is too restrictive and does not allow us to explore the entire parameter space.

More generally, we can consider carrying out a similar procedure for the full two-channel model Eq. (1), both in the continuum (see App. B) and on a lattice (see App. C). Since on a lattice the effective masses of the atom and molecules need no longer be coupled, we find that linearising the lattice two-channel model leads to the Q3WI model with velocities u, v_1, v_2 and detuning ν that can be tuned independently. Hence, this procedure allows us to access all of the regimes of the Q3WI model that we find.

Summary of main results: In this paper, we use the coordinate Bethe Ansatz to find the exact ground state for the Q3WI Hamiltonian, given by Eq. (3). We find that, as is usual in the Bethe Ansatz, the ground state is parametrized by the momenta of the atoms; the molecules, however, only enter the problem through their velocity u and the detuning ν . In the thermodynamic limit, we derive a set of coupled integral equations for the excitation spectrum of the system. In general, these can only be solved numerically, except in the strongly and weakly interacting limits, which we proceed to study. For strong interactions, the system reduces to that of non-interacting Fermi gases, in a way similarly to strongly interacting Fermi or Bose gases in 1D [38, 39].

In the more interesting limit of weak interactions, we find that the nature of the solution is primarily determined by the speed of the molecules relative to that of the atoms i.e., the case where u is greater or less than both v_1 and v_2 differs qualitatively from the case where $v_1 > u > v_2$. In the former case, we find that while the excitation spectra of the atoms remain gapless piecewise linear functions of momenta, there are certain parameter regimes where the fermions display unconventional behavior. For instance, they can remain interacting deep within the Fermi sea—all the way down to a large momentum cut-off (imposed since the spectrum is unbounded)—or the chirality of the slower moving atoms can change due to the weak interactions.

In the latter case (where $v_1 > u > v_2$), we find that the system, in the limit of weak coupling, behaves similarly to the weakly interacting Bose gas. The fact that fermions can behave in this manner is not by itself surprising—it has been known for quite some time that 1D spinless fermions interacting via a specially chosen two-body potential can be mapped exactly onto an interacting Bose gas, and in particular, can be in its weakly interacting regime [40–42]. This is similar to the regime our model displays in the case when $v_1 > u > v_2$. We term this the “quasi-condensate” regime of the Q3WI model, in which the spectrum is no longer linear but is still gapless. The wide variety of behaviors exhibited by the Q3WI model reflects the fact that even weak interactions in 1D may significantly alter the nature of the ground state and of low lying excitations.

In all cases but one (where $v_1 > 0 > v_2$ and u lies between the two) we are able to construct the leading order solution for the ground state densities and excitation spectra, from which we calculate the compressibilities. Being discontinuous as functions of the densities, they indicate that the system undergoes quantum phase transitions. In all cases, the transition is from a phase where, near the Fermi momentum, the system goes from being effectively interacting to non-interacting (or vice-versa).

The rest of the paper is organized as follows: In Sec. II, we construct the exact many-body wave-function for the Q3WI Hamiltonian using the coordinate Bethe Ansatz and argue that there are no bound states in this problem. We then derive the Bethe Ansatz equations by imposing periodic boundary conditions. In Sec. III, we take the thermodynamic limit of these equations and derive a set of coupled integral (known as the Thermodynamic Bethe Ansatz (TBA)) equations that describe the ground state densities and excitation spectra of the system at zero temperature. In Sec. IV, we consider the limit of infinite interaction strength.

In Sec. V, we discuss the case of weak interactions qualitatively. In Sec. VI we describe the regime where the molecular velocity is greater than or less than that of the atoms ($u < \text{or} > v_1, v_2$). Here, we keep only the leading order, δ -function term in the integral kernel for the TBA equations in order to derive the leading order solution for the ground state densities and excitation spectra in

the $T \rightarrow 0$ limit. Moreover, we show that in all possible regimes, the system undergoes a quantum phase transition.

In Sec. VII, we describe the case where $v_1 > u > v_2$. In this case, as the densities diverge in the limit where g goes to zero, we have to consider the next order term in the interaction strength g . For the case where atomic velocities have the same sign, we find the leading order solution for the ground state densities at $T = 0$ and derive the excitation spectra. As in the previous case, we find that the system exhibits a quantum phase transition.

II. BETHE ANSATZ FOR THE Q3WI

The Hamiltonian for our model is given by Eq. (3). In this model, as is always the case in the presence of a Feshbach resonance, the total number of fermions, N_f , is not conserved but the total atomic numbers

$$N_1 = N_{f1} + N_b, \quad N_2 = N_{f2} + N_b, \quad (5)$$

where

$$N_{f\sigma} = \int dx \hat{a}_\sigma^\dagger(x) \hat{a}_\sigma(x), \quad N_b = \int dx \hat{b}^\dagger(x) \hat{b}(x), \quad (6)$$

are conserved. We note that in what follows, we will always work in the regime where $v_1 \neq v_2$ i.e., we will never allow the particles to have equal velocities (the case of equal velocities $v_1 = v_2$ is highly degenerate and in principle could be considered separately).

Consider the following wave function in the sector where $N_1 = 1, N_2 = 1$,

$$|\Psi\rangle_{1,1} = \int dx dy \psi(x, y) \hat{a}_1^\dagger(x) \hat{a}_2^\dagger(y) |0\rangle + \int dR \phi(R) \hat{b}^\dagger(R) |0\rangle, \quad (7)$$

where $|0\rangle$ denotes the Fock vacuum. This leads to the following Schrödinger equation

$$-i \left(v_1 \frac{\partial}{\partial x} + v_2 \frac{\partial}{\partial y} \right) \psi(x, y) + g \phi(x) \delta(x - y) = E \psi(x, y), \quad (8)$$

$$\left(\nu - iu \frac{\partial}{\partial R} \right) \phi(R) + g \psi(R, R) = E \phi(R). \quad (9)$$

The linear spectrum only allows for a solution in the form

$$\psi(x, y) = (\theta(y - x) + S\theta(x - y)) e^{ik_1 x + ik_2 y}, \quad (10)$$

where $\theta(x)$ is the usual Heaviside function with $\theta(0) = \frac{1}{2}$. It is worth noting that due to the linear free particle spectrum, the wave function is a discontinuous function of the position variables at $g \neq 0$. This is in contrast with the usual case of a particle with a conventional kinetic energy—quadratic in momentum—moving in a

delta-function potential, where the wave function is continuous.

Solving these equations, with $E = k_1 v_1 + k_2 v_2$, we find

$$\phi(x) = \frac{g(1+S)}{2(E+\nu-u(k_1+k_2))} e^{i(k_1+k_2)x}, \quad (11)$$

from which we find the S -matrix

$$S(k_1, k_2) = \frac{\frac{-ig^2}{2(v_1-v_2)} + v_1 k_1 + v_2 k_2 - u(k_1+k_2) - \nu}{\frac{ig^2}{2(v_1-v_2)} + v_1 k_1 + v_2 k_2 - u(k_1+k_2) - \nu}. \quad (12)$$

As required by unitarity, $SS^* = 1$. We also see that $\lim_{k_1 \rightarrow k_2} S = -1$, i.e., at low energies (relative momentum, $q = (k_1 - k_2)/2 \rightarrow 0$), the fermions undergo total reflection. This is in accordance with a general result stated in [32]. Note that we can alternatively derive the same S -matrix by using the T -matrix formalism (see App. A). The T -matrix formalism has the advantage of automatically resolving the ambiguity built into the choice of the value for $\theta(0)$.

If we could find $k_1 = q_1 + i\epsilon_1$ and $k_2 = q_2 - i\epsilon_2$, with $\epsilon_{1,2} > 0$, such that $S = \infty$, then there would exist bound states in this model. However, we need $v_1 \epsilon_1 = v_2 \epsilon_2$ in order to keep the energy of the state real, and demanding that $\phi(x)$, given by Eq. (11), be normalizable imposes the condition $\epsilon_1 = \epsilon_2$. Thus, since we are considering the case where $v_1 \neq v_2$, there exist no bound states in our problem.

Until the end of this section, let us label the momenta of the v_1 particles as $k_j^{(1)}$ and that of the v_2 particles as $k_j^{(2)}$, where j numbers the particles. Then, following the theory of integrable systems [43], we can construct the most general eigenstate of the Hamiltonian Eq. (3),

$$|\Psi\rangle_{N_1, N_2} = \int \prod_{i=1}^{N_1} dx_i \prod_{i=1}^{N_2} dy_i \psi(x_1, \dots, x_{N_1}; y_1, \dots, y_{N_2}) \times \hat{a}_1^\dagger(x_1) \dots \hat{a}_{N_1}^\dagger(x_{N_1}) \hat{a}_2^\dagger(y_1) \dots \hat{a}_{N_2}^\dagger(y_{N_2}) |0\rangle + \dots, \quad (13)$$

where ψ is given by

$$\psi(x_1, \dots, x_{N_1}; y_1, \dots, y_{N_2}) = \mathcal{A} \prod_{j=1}^{N_1} e^{ik_j^{(1)} x_j} \prod_{j=1}^{N_2} e^{ik_j^{(2)} y_j} \times \prod_{m,n} \left[\theta(y_m - x_n) + \theta(x_n - y_m) S(k_n^{(1)}, k_m^{(2)}) \right] \quad (14)$$

where \mathcal{A} denotes anti-symmetrization over all x_j and over all y_j . The dots at the end of Eq. (13) stand for terms where pairs of fermions are replaced by bosons, in analogy with Eq. (7).

It is straightforward to check that Eq. (13) is indeed an eigenstate with energy

$$E = v_1 \sum_{j=1}^{N_1} k_j^{(1)} + v_2 \sum_{j=1}^{N_2} k_j^{(2)}. \quad (15)$$

Crucial in this verification is the fact that the Q3WI Hamiltonian only includes first derivatives of the annihilation operators, unlike standard Hamiltonians, such as Eq. (1), which involve second derivatives of the annihilation operators. As a result, the three particle terms which typically need to cancel for a one-dimensional problem to be integrable are absent in our problem.

Imposing periodic boundary conditions, with L the system size, we deduce the Bethe-Ansatz equations

$$e^{ik_j^{(1)} L} \prod_{m=1}^{N_2} \frac{k_j^{(1)}(v_1 - u) + k_m^{(2)}(v_2 - u) - \nu - i \frac{g^2}{2(v_1 - v_2)}}{k_j^{(1)}(v_1 - u) + k_m^{(2)}(v_2 - u) - \nu + i \frac{g^2}{2(v_1 - v_2)}} = 1, \\ e^{ik_j^{(2)} L} \prod_{m=1}^{N_1} \frac{k_m^{(1)}(v_1 - u) + k_j^{(2)}(v_2 - u) - \nu + i \frac{g^2}{2(v_1 - v_2)}}{k_m^{(1)}(v_1 - u) + k_j^{(2)}(v_2 - u) - \nu - i \frac{g^2}{2(v_1 - v_2)}} = 1. \quad (16)$$

Taking the logarithm, we find

$$k_j^{(1)} = \frac{2\pi}{L} I_j - \frac{2}{L} \sum_{m=1}^{N_2} \tan^{-1} \left(\frac{k_j^{(1)}(v_1 - u) + k_m^{(2)}(v_2 - u) - \nu}{\frac{g^2}{2(v_1 - v_2)}} \right), \\ k_j^{(2)} = \frac{2\pi}{L} J_j + \frac{2}{L} \sum_{m=1}^{N_1} \tan^{-1} \left(\frac{k_m^{(1)}(v_1 - u) + k_j^{(2)}(v_2 - u) - \nu}{\frac{g^2}{2(v_1 - v_2)}} \right), \quad (17)$$

where the I_j (J_j) are distinct half-integers if N_1 (N_2) is odd, and distinct integers if N_1 (N_2) is even. We can thus parametrize the solutions to the Bethe equations by sets of integers I_j and J_j , which act as quantum numbers for the momenta, $k^{(1)}$ and $k^{(2)}$ respectively. The existence of a unique solution is proved in Ref. [44], where it is demonstrated that the action corresponding to these equations is bounded below and always has a unique minimum in the thermodynamic limit, which we now proceed to study.

III. THERMODYNAMICS AND EXCITATION SPECTRUM

We are now interested in taking the thermodynamic limit of the Bethe Ansatz equations derived in the previous section. To this end, we promote I_j and J_j to continuous variables I and J , with $k^{(1)}$ and $k^{(2)}$ now becoming functions of I and J respectively, rather than being labelled by a subscript indicating a particle number. Henceforth, it will be convenient to change notations $k^{(1)} \rightarrow k_1$, $k^{(2)} \rightarrow k_2$, with k_1 and k_2 simply denoting the momenta of each species of fermionic particles.

We then differentiate the Bethe Ansatz equations with respect to the momenta k_1 and k_2 , and introduce the density of vacancies (where a full vacancy is a particle and an empty one is a hole) for the k_1 and k_2 particles

$$\rho_1^t(k_1) = \frac{1}{L} \frac{dI}{dk_1}, \quad \rho_2^t(k_2) = \frac{1}{L} \frac{dJ}{dk_2}, \quad (18)$$

where $\rho_1^t(k_1) = \rho_1(k_1) + \rho_1^h(k_1)$ and $\rho_2^t(k_2) = \rho_2(k_2) + \rho_2^h(k_2)$, with $\rho_{1,2}$ and $\rho_{1,2}^h$ denoting the densities of full and empty vacancies of each particle species respectively. This leads to the following set of coupled integral equations for the densities

$$\begin{aligned}\rho_1^t(k_1) &= \frac{1}{2\pi} - \frac{u-v_1}{2\pi} \int dk_2 \rho_2(k_2) K(k_1, k_2), \\ \rho_2^t(k_2) &= \frac{1}{2\pi} + \frac{u-v_2}{2\pi} \int dk_1 \rho_1(k_1) K(k_1, k_2),\end{aligned}\quad (19)$$

where we have defined the integral kernel,

$$K(k_1, k_2) = \frac{4g^2(v_1 - v_2)}{g^4 + 4(v_1 - v_2)^2 (k_1(u - v_1) + k_2(u - v_2) + \nu)^2}.$$

Since the energy of the fermions is unbounded below owing to their chiral nature, we have to implement momentum cut-offs. If, for instance, v_1, v_2 are both positive, these cut-offs can be implemented in the following way,

$$\begin{aligned}\rho_1^t(k_1) &= \frac{1}{2\pi} - \frac{u-v_1}{2\pi} \int_{-\Lambda}^{\infty} dk_2 \rho_2(k_2) K(k_1, k_2), \\ \rho_2^t(k_2) &= \frac{1}{2\pi} + \frac{u-v_2}{2\pi} \int_{-\Lambda}^{\infty} dk_1 \rho_1(k_1) K(k_1, k_2).\end{aligned}\quad (21)$$

Here, the cut-off Λ removes particles with large negative kinetic energies. If v_1 is negative, we instead cut-off large positive momenta k_1 , and similarly, if $v_2 < 0$, we cut-off large positive momenta k_2 .

To determine the ground state and excitation spectrum of the system, we follow the method introduced by Yang and Yang [45], where we first find the excitation spectrum at finite temperature and then take the limit $T \rightarrow 0$ (see [43, 46] for a review).

The total number of particles of type v_1 and v_2 can be found by integrating the density functions

$$N_1/L = \int dk_1 \rho_1(k_1), \quad N_2/L = \int dk_2 \rho_2(k_2), \quad (22)$$

while the total energy of the system is given by

$$E/L = v_1 \int dk_1 \rho_1(k_1) k_1 + v_2 \int dk_2 \rho_2(k_2) k_2. \quad (23)$$

The entropy of the system is

$$\begin{aligned}S/L &= \int dk_1 [\rho_1^t \log(\rho_1^t) - \rho_1 \log(\rho_1) - \rho_1^h \log(\rho_1^h)] + \\ &\int dk_2 [\rho_2^t \log(\rho_2^t) - \rho_2 \log(\rho_2) - \rho_2^h \log(\rho_2^h)].\end{aligned}\quad (24)$$

We introduce the thermodynamic potential $\Omega = E - TS - h_1 N_1 - h_2 N_2$, where T is the temperature, and h_1 and h_2 are the chemical potentials conjugate to the conserved particle numbers N_1 and N_2 , defined in Eq. (5). We then minimize Ω with respect to ρ_1 and ρ_2 , recalling that

$$\begin{aligned}\delta \rho_1^t(k_1) &= -\frac{u-v_1}{2\pi} \int dk_2 K(k_1, k_2) \delta \rho_2(k_2), \\ \delta \rho_2^t(k_2) &= \frac{u-v_2}{2\pi} \int dk_1 K(k_1, k_2) \delta \rho_1(k_1),\end{aligned}\quad (25)$$

and find a system of coupled non-linear integral equations, usually called the Thermodynamic Bethe Ansatz (TBA) equations,

$$\begin{aligned}\epsilon_1(k_1) &= k_1 v_1 - h_1 \\ &\quad - T \frac{u-v_2}{2\pi} \int dk_2 K(k_1, k_2) \ln(1 + e^{-\frac{\epsilon_2(k_2)}{T}}), \\ \epsilon_2(k_2) &= k_2 v_2 - h_2 \\ &\quad + T \frac{u-v_1}{2\pi} \int dk_1 K(k_1, k_2) \ln(1 + e^{-\frac{\epsilon_1(k_1)}{T}}).\end{aligned}\quad (26)$$

Here, following [43] we have defined

$$\frac{\rho_1^h(k_1)}{\rho_1(k_1)} = e^{\frac{\epsilon_1(k_1)}{T}}, \quad \frac{\rho_2^h(k_2)}{\rho_2(k_2)} = e^{\frac{\epsilon_2(k_2)}{T}}, \quad (27)$$

with $\epsilon_1(k_1)$ and $\epsilon_2(k_2)$ playing the role of the excitation spectrum of the v_1 and v_2 particles respectively. In principle, this set of equations produces the excitation spectrum of the system, but being non-linear, there exists no analytic solution.

Since we are interested in the zero temperature limit here, taking $T \rightarrow 0$ we find that

$$\begin{aligned}\epsilon_1(k_1) &= k_1 v_1 - h_1 + \frac{u-v_2}{2\pi} \int_{\epsilon_2(k_2) < 0} dk_2 K(k_1, k_2) \epsilon_2(k_2), \\ \epsilon_2(k_2) &= k_2 v_2 - h_2 - \frac{u-v_1}{2\pi} \int_{\epsilon_1(k_1) < 0} dk_1 K(k_1, k_2) \epsilon_1(k_1).\end{aligned}\quad (28)$$

Here, the integrals are restricted over the regions where $\epsilon_1(k_1), \epsilon_2(k_2) < 0$. In addition, from Eq. (27) we see that in the zero temperature limit,

$$\begin{aligned}\epsilon < 0 &\implies \rho^h = 0, \\ \epsilon > 0 &\implies \rho = 0,\end{aligned}\quad (29)$$

with the Fermi-momenta, k_1^f, k_2^f , defined in such a way that

$$\epsilon_1(k_1 = k_1^f) = 0, \quad \epsilon_2(k_2 = k_2^f) = 0. \quad (30)$$

From these definitions, we see that if $\epsilon(k) > 0$, then the excitation corresponds to a particle; otherwise, it corresponds to a hole with energy $-\epsilon(k)$.

For an arbitrary interaction strength g , these equations can only be solved numerically, but in what follows we develop analytic solutions for the limits of infinite and weak interactions at zero temperature.

IV. STRONGLY INTERACTING REGIME

The strongly interacting regime of the Q3WI model corresponds to the broad resonance regime and is accessed by taking the limit $g, \nu \rightarrow \infty$, while keeping the ratio $g^2/\nu = \gamma$ fixed. In this limit, we can integrate

out the bosonic molecules b , and the Q3WI Hamiltonian (Eq. (3)) reduces to

$$\hat{H} = \int dx \left[\sum_{\sigma=1,2} \hat{a}_{\sigma}^{\dagger} (-iv_{\sigma} \partial_x) \hat{a}_{\sigma} - \gamma \hat{a}_1^{\dagger} \hat{a}_2^{\dagger} \hat{a}_2 \hat{a}_1 \right]. \quad (31)$$

We note that in the conventional case with quadratic dispersion Eq. (2), this limit is conventionally referred to as the limit of broad resonance, with the term “strong interactions” reserved for the case when $|\gamma|$ is large. We will see however that in our case, where particles disperse linearly, the physics of Eq. (31) does not depend much on the magnitude of γ ; we thus refer to Eq. (31) with arbitrary γ as the strongly interacting regime.

Hence, in the strongly interacting regime, the Q3WI model describes two species of chiral fermions interacting through a short ranged δ -function interaction, whose strength γ is controlled by the parameters g, ν of the original resonant system. Given the simplicity of this limit, we first study the model Eq. (31) directly and then check that the Bethe Ansatz solution developed in the previous section indeed reproduces this limit correctly.

In order to study the scattering of two different species of fermions (since Fermi statistics prevent two particles of the same species from interacting), we consider the two-particle wave function

$$|\Psi\rangle_2 = \int dx dy \psi(x, y) \hat{a}_1^{\dagger}(x) \hat{a}_2^{\dagger}(y) |0\rangle. \quad (32)$$

This leads to the Schrödinger equation

$$\left(-iv_1 \frac{\partial}{\partial x} - iv_2 \frac{\partial}{\partial y} \right) \psi(x, y) - \gamma \delta(x-y) \psi(x, y) = E \psi(x, y). \quad (33)$$

Since \hat{a}_1^{\dagger} and \hat{a}_2^{\dagger} describe distinguishable species of chiral fermions, we should not expect the solution to obey any particular symmetries. Indeed, the solution to Eq. (33) is

$$\psi(x, y) = e^{ik_1 x + ik_2 y} (\theta(y-x) + S \theta(x-y)), \quad (34)$$

where the energy $E = k_1 v_1 + k_2 v_2$. Integrating Eq. (33) over the range $x = y \pm \epsilon$, we find that

$$\lim_{\epsilon \rightarrow 0} (-iv_1 + iv_2) \psi(x, y)|_{x=y+\epsilon}^{x=y-\epsilon} = \gamma \psi(x, y)|_{x=y}, \quad (35)$$

which leads to the S -matrix

$$S = \frac{2(v_1 - v_2) + i\gamma}{2(v_1 - v_2) - i\gamma}. \quad (36)$$

Interestingly, this S -matrix is completely independent of momenta. Since $S = e^{i\theta}$ is described by a constant phase shift, it demonstrates that the only effect of the short range δ -function potential on the scattering of chiral fermions is to shift the phase of the outgoing wave relative to the incoming wave, regardless of whether the interaction is repulsive or attractive.

Another interesting feature of this solution is that both the limit $\gamma \rightarrow 0$ and $\gamma \rightarrow \infty$ describe two species of non-interacting fermions. In particular,

$$\lim_{\gamma \rightarrow 0} S = 1, \quad (37)$$

so that the solution to Eq. (33) becomes

$$\psi(x, y) = e^{ik_1 x + ik_2 y}. \quad (38)$$

Since $\psi(x, x) \neq 0$ and since the particles are allowed to occupy the same momentum state, the limit $\gamma \rightarrow 0$ clearly describes two distinct species of non-interacting fermions. Similarly, in the opposite limit

$$\lim_{\gamma \rightarrow \pm\infty} S = -1, \quad (39)$$

so that Eq. (33) is solved by

$$\psi(x, y) = e^{ik_1 x + ik_2 y} (\theta(y-x) - \theta(x-y)). \quad (40)$$

In this case, $\psi(x, x) = 0$ but the particles are still allowed to occupy the same momentum state. Thus, in this regime, regardless of whether the interaction is attractive or repulsive, Eq. (31) describes two non-interacting Fermi-gases. This is reflected in the fact that the S -matrix is momentum-independent.

Since we have at our disposal the Bethe ansatz solutions Eq. (16) to the full Q3WI model Eq. (3), it is instructive to verify that they indeed reproduce the broad resonance regime discussed above. First, we observe that in the limit $g^2/\nu \rightarrow \gamma$, Eq. (12) reduces to Eq. (36), reproducing the constant S -matrix as expected. We thus find that the Bethe ansatz equations reduce to

$$\begin{aligned} k_j^{(1)} &= \frac{2\pi}{L} I_j + \frac{2N_2}{L} \tan^{-1} \left(\frac{2(v_1 - v_2)}{\gamma} \right), \\ k_j^{(2)} &= \frac{2\pi}{L} J_j - \frac{2N_1}{L} \tan^{-1} \left(\frac{2(v_1 - v_2)}{\gamma} \right), \end{aligned} \quad (41)$$

from which we deduce the densities of the chiral fermions in the broad resonance regime,

$$\rho_1^t(k_1) = \rho_2^t(k_2) = \frac{1}{2\pi}, \quad \forall \gamma. \quad (42)$$

Similarly, if we now consider Eqs. (26) in this limit, the integral kernel vanishes, leading to the excitation spectra

$$\begin{aligned} \epsilon_1(k_1) &= k_1 v_1 - h_1, \\ \epsilon_2(k_2) &= k_2 v_2 - h_2, \end{aligned} \quad (43)$$

from which we can deduce the finite temperature densities of the fermions,

$$\begin{aligned} \rho_1(k_1) &= \frac{1}{2\pi} \frac{1}{e^{\frac{k_1 v_1 - h_1}{T}} + 1}, \\ \rho_2(k_2) &= \frac{1}{2\pi} \frac{1}{e^{\frac{k_2 v_2 - h_2}{T}} + 1}. \end{aligned} \quad (44)$$

We recognize in these two independent Fermi-Dirac distributions.

Thus, unlike the usual case of non-chiral fermions with quadratic dispersion, where at infinite repulsion the fermions behave as a single non-interacting species [46], here we find that the strongly interacting (or broad resonance) regime corresponds to both species of fermions surviving and becoming completely non-interacting. In particular, the short ranged δ -function interaction between the two species amounts to a constant scattering amplitude, which leaves the dispersion completely unchanged, with no renormalization of their velocities.

V. WEAKLY INTERACTING REGIME

The weakly interacting limit of the Q3WI model Eq. (3) corresponds to the limit $g \rightarrow 0$. The system is described by the Bethe Ansatz solutions developed in Sec. III, where the integral kernel (20) in this limit reduces to

$$K(k_1, k_2) = 2\pi \operatorname{sgn}(v_1 - v_2) \delta(k_1(u - v_1) + k_2(u - v_2) + \nu) + \frac{g^2}{v_1 - v_2} \frac{1}{(k_1(u - v_1) + k_2(u - v_2) + \nu)^2} + O(g^4). \quad (45)$$

The leading order (g -independent) term of the integral kernel clearly depends on the relative velocities of the chiral fermions v_1 and v_2 , but it also depends on the relative strength of the bosonic velocity u through the δ -function. Owing to this, we find that there are two distinct regimes that must be separately analyzed

A. $u > v_1 > v_2$,

B. $v_1 > u > v_2$.

Here, we assume without loss of generality that $v_1 > v_2$ since the cases where $v_2 > v_1$ simply involve an exchange of fermions of type 1 and 2. Furthermore, the parity $x \rightarrow -x$ transformation changes the sign of all three velocities u , v_1 , and v_2 , so that cases such as $v_1 > v_2 > u$ can be obtained from case A by a combination of parity and fermion type exchange.

For each of these cases, we are interested in understanding the ground state properties and excitation spectra of the chiral fermions in the zero temperature limit. We consider case A in Sec. VI. We find that the leading order behavior of the excitation spectra Eq. (26) at finite T can be established by considering only the δ -function term in the integral kernel $K(k_1, k_2)$. From these, we can establish a finite T solution for the densities, with the ground state densities found by taking the limit $T \rightarrow 0$ (despite what one might naïvely assume, solving the Bethe Ansatz equations in this case directly at $T = 0$ is more difficult than working at $T > 0$ and then taking the limit $T \rightarrow 0$). We find that the excitation spectra of the chiral fermions are piece-wise linear

functions of momenta. Our procedure then allows us to identify and describe several phases and phase transitions in our system.

For case B, considered in Sec. VII, where the molecular velocity is bracketed by that of the atoms, we find that simply considering the δ -function term is insufficient and that we must also account for the $O(g^2)$ term to establish the leading order solution (which is why the $O(g^2)$ term was retained in Eq. (45)). In this case, in order to find the excitation spectra analytically, we make an ansatz that the excitation spectra change sign only once. This ansatz gives us a consistent solution only in the cases where v_1 and v_2 have the same sign. The solution to the Bethe Ansatz equations found via our procedure is reminiscent of the solution to similar equations that describe the weakly interacting Bose gas, which is in a regime resembling Bose condensation. In particular, the weakly interacting Bose gas can be described with good accuracy by the classical one-dimensional Gross-Pitaevskii (non-linear Schrödinger) equation despite the formal absence of Bose condensation in one-dimensional space. Since our solution for the Q3WI model in case B closely resembles this behavior, we term the phase in case B the “quasi-condensate” phase of our model.

For the case where the atomic velocities have opposite signs while the molecular velocity lies between them, we were not able to find an analytic solution since our ansatz leads to a physically inconsistent solution.

VI. LINEAR, GAPLESS BEHAVIOR AT WEAK INTERACTIONS (CASE A)

We first study the cases where the molecular velocity is greater than that of the chiral fermions. Specifically, we consider case A, which corresponds to $u > v_1 > v_2$. In order to study this regime, we first define the reduced integral kernel

$$\tilde{K}(k_1, k_2) = \lim_{g \rightarrow 0} K(k_1, k_2) = 2\pi \delta(k_1(u - v_1) + k_2(u - v_2) + \nu), \quad (46)$$

since it is sufficient to replace K by its limiting $g \rightarrow 0$ value to find the ground state properties of the Q3WI model at weak interaction strengths within this regime. The TBA equations (27) are thus

$$\begin{aligned} \epsilon_1(k_1) &= k_1 v_1 - h_1 \\ &\quad - T \frac{(u - v_2)}{2\pi} \int dk_2 \tilde{K}(k_1, k_2) \log(1 + e^{-\frac{\epsilon_2(k_2)}{T}}), \\ \epsilon_2(k_2) &= k_2 v_2 - h_2 \\ &\quad + T \frac{(u - v_1)}{2\pi} \int dk_1 \tilde{K}(k_1, k_2) \log(1 + e^{-\frac{\epsilon_1(k_1)}{T}}), \end{aligned} \quad (47)$$

while the densities satisfy the coupled integral equations

$$\begin{aligned}\rho_1^t(k_1) &= \frac{1}{2\pi} - \frac{(u-v_1)}{2\pi} \int dk_2 \rho_2(k_2) \tilde{K}(k_1, k_2), \\ \rho_2^t(k_2) &= \frac{1}{2\pi} + \frac{(u-v_2)}{2\pi} \int dk_1 \rho_1(k_1) \tilde{K}(k_1, k_2).\end{aligned}\quad (48)$$

We have to supplement the integrals with a momentum cut-off $\Lambda \gg 1$, since the energies are unbounded from below (above) if v_i is positive (negative). Since we are working with the reduced kernel \tilde{K} , Eqs. (47) simplify,

$$\begin{aligned}\epsilon_1(k_1) &= k_1 v_1 - h_1 \\ &\quad - T \log \left(1 + \exp \left(-\frac{\epsilon_2 \left(-\frac{k_1(u-v_1)+\nu}{u-v_2} \right)}{T} \right) \right), \\ \epsilon_2(k_2) &= k_2 v_2 - h_2 \\ &\quad + T \log \left(1 + \exp \left(-\frac{\epsilon_1 \left(-\frac{k_2(u-v_2)+\nu}{u-v_1} \right)}{T} \right) \right).\end{aligned}\quad (49)$$

This is valid for arbitrary k_1 and k_2 . In order to simplify these equations further, we set

$$\tilde{k}_2 = -\frac{k_1(u-v_1)+\nu}{u-v_2}, \quad (50)$$

and find that

$$\begin{aligned}\epsilon_1(k_1) &= k_1 v_1 - h_1 - T \log \left(1 + \exp \left(-\frac{\epsilon_2(\tilde{k}_2)}{T} \right) \right), \\ \epsilon_2(\tilde{k}_2) &= \tilde{k}_2 v_2 - h_2 + T \log \left(1 + \exp \left(-\frac{\epsilon_1(k_1)}{T} \right) \right).\end{aligned}\quad (51)$$

Equivalently,

$$e^{-\frac{\epsilon_1(k_1)}{T}} = e^{-\frac{k_1 v_1 - h_1}{T}} \left(1 + \frac{\exp \left(\frac{\frac{k_1(u-v_1)+\nu}{u-v_2} v_2 + h_2}{T} \right)}{1 + e^{-\frac{\epsilon_1(k_1)}{T}}} \right). \quad (52)$$

Solving this quadratic equation for $\exp(-\epsilon_1(k_1)/T)$ leads to

$$\exp \left(-\frac{\epsilon_1(k_1)}{T} \right) = \frac{1}{2} \left(\exp \left(-\frac{k_1 v_1 - h_1}{T} \right) - 1 \right) + \frac{1}{2} \sqrt{\left(\exp \left(-\frac{k_1 v_1 - h_1}{T} \right) + 1 \right)^2 + 4 \exp \left(-\frac{k_1 v_1 - \frac{k_1(u-v_1)+\nu}{u-v_2} v_2 - h_1 - h_2}{T} \right)}. \quad (53)$$

Here, we must choose the positive sign in front of the square root in order to keep the whole expression positive. This gives us the finite temperature solution for the excitation spectrum $\epsilon_1(k_1)$ of the first species of chiral fermions. The spectrum $\epsilon_2(k_2)$ of the second species of fermions can then be found by substituting Eq. (53) back into the equation for $\epsilon_2(k_2)$.

Since we have established the finite temperature solution for the spectra, we can also find the solutions for the densities from Eq. (48). Recalling that $\rho_i^t = \rho_i + \rho_i^h$ and using Eq. (27), these simplify to

$$\begin{aligned}\rho_1(k_1) \left(1 + e^{\frac{\epsilon_1(k_1)}{T}} \right) &= \frac{1}{2\pi} - \frac{u-v_1}{u-v_2} \rho_2 \left(-\frac{k_1(u-v_1)+\nu}{u-v_2} \right), \\ \rho_2(k_2) \left(1 + e^{\frac{\epsilon_2(k_2)}{T}} \right) &= \frac{1}{2\pi} + \frac{u-v_2}{u-v_1} \rho_1 \left(-\frac{k_2(u-v_2)+\nu}{u-v_1} \right).\end{aligned}\quad (54)$$

These are a set of simple algebraic equations which can

be solved in order to find that

$$\begin{aligned}\rho_1(k_1) &= \frac{\frac{1}{2\pi} \left(1 + \exp \left(\frac{\epsilon_2 \left(-\frac{k_1(u-v_1)+\nu}{u-v_2} \right)}{T} \right) \right) - \frac{1}{2\pi} \frac{u-v_1}{u-v_2}}{1 + \left(1 + \exp \left(\frac{\epsilon_2 \left(-\frac{k_1(u-v_1)+\nu}{u-v_2} \right)}{T} \right) \right) \left(1 + \exp \left(\frac{\epsilon_1(k_1)}{T} \right) \right)}, \\ \rho_2(k_2) &= \frac{\frac{1}{2\pi} \left(1 + \exp \left(\frac{\epsilon_1 \left(-\frac{k_2(u-v_2)+\nu}{u-v_1} \right)}{T} \right) \right) + \frac{1}{2\pi} \frac{u-v_2}{u-v_1}}{1 + \left(1 + \exp \left(\frac{\epsilon_1 \left(-\frac{k_2(u-v_2)+\nu}{u-v_1} \right)}{T} \right) \right) \left(1 + \exp \left(\frac{\epsilon_2(k_2)}{T} \right) \right)}.\end{aligned}\quad (55)$$

Equations (53), (55) are the solutions to the Bethe Ansatz equations at finite T in case A, studied in this section.

In order to uncover the physics described by these equations, we now examine the $T \rightarrow 0$ limit of the expressions we have obtained thus far. Technically, this limit is simple to take. It follows from observing that $\exp(c/T) \gg 1$ in this limit if $c > 0$ and $\exp(c/T) \ll 1$ if $c < 0$. The procedure then reduces to evaluating the

signs of various combinations of parameters; upon doing this, the problem splits into various cases distinguished by different values of these signs.

Carrying out this procedure, we find that there are five further cases within case A, $u > v_1 > v_2$, that must be considered separately,

1. $u > v_1 > v_2 > 0$,

2. $u > v_1 > 0 > v_2$:

- 2i) $u < \frac{2v_1v_2}{v_1+v_2}$,

- 2ii) $u > \frac{2v_1v_2}{v_1+v_2}$,

3. $u > 0 > v_1 > v_2$,

4. $0 > u > v_1 > v_2$.

We now discuss the general procedure through which the ground state properties of these systems can be derived, using as an example the case A1 where $u > v_1 > v_2 > 0$. In particular, we will establish the presence of a quantum phase transition in the Q3WI model through this example and leave the details of the transitions in the other cases to App. D, since the same method applies to each of these.

Quantum phase transition in the Q3WI model

As a first step in establishing the ground state properties of the Q3WI model in the weakly interacting limit, we consider particle velocities such that $u > v_1 > v_2 > 0$ and take the zero temperature limit $T \rightarrow 0$ of Eq. (53). This gives us the excitation spectra and ground state densities of the chiral fermions. For both species of fermions, the excitation spectra turn out to be piece-wise linear functions of momenta, with derivatives $\epsilon'_i(k_i)$ that are discontinuous at certain momenta $k_i^{(j)}$ ($j = a, b, c$). For future reference, these are defined as

$$\begin{aligned} k_1^{(a)} &= \frac{(h_1 - h_2)(u - v_2) - \nu v_2}{u(v_1 + v_2) - 2v_1v_2}, \\ k_1^{(b)} &= \frac{(h_1 + h_2)(u - v_2) + \nu v_2}{u(v_1 - v_2)}, \\ k_1^{(c)} &= \frac{h_2(v_2 - u) - \nu v_2}{v_2(u - v_1)}, \\ k_2^{(a)} &= -\frac{(h_1 + h_2)(u - v_1) + \nu v_1}{u(v_1 - v_2)}, \\ k_2^{(b)} &= \frac{(h_2 - h_1)(u - v_1) - \nu v_1}{u(v_1 + v_2) - 2v_1v_2}, \\ k_2^{(c)} &= \frac{h_1(v_1 - u) - \nu v_1}{v_1(u - v_2)}. \end{aligned} \quad (56)$$

Furthermore, the ground state densities $\rho_i(k_i)$ are momentum-independent constants that change their values discontinuously at the above momenta $k_i^{(j)}$.

We further find that the behavior of the excitation spectra and ground state densities differs depending on the sign of the parameter

$$\alpha(h_1, h_2, \nu) = h_1v_2(u - v_1) + h_2v_1(u - v_2) + \nu v_1v_2, \quad (57)$$

which is controlled by the chemical potentials h_i and the detuning ν . We note that at $\alpha(h_1, h_2) = 0$, the momenta defined in Eq. (56) satisfy $k_i^{(a)} = k_i^{(b)} = k_i^{(c)}$.

For $\alpha \leq 0$, the excitation spectra are

$$\epsilon_1(k_1) = \quad (58)$$

$$\begin{cases} k_1v_1 - h_1, & k_1 < k_1^{(c)}, \\ \frac{k_1u(v_1 - v_2) - \nu v_2}{u - v_2} - h_1 - h_2, & k_1 > k_1^{(c)}, \end{cases} \quad (59)$$

$$\epsilon_2(k_2) = \quad (60)$$

$$\begin{cases} k_2v_2 - h_2, & k_2 < k_2^{(c)}, \\ \frac{k_2(u(v_1 + v_2) - 2v_1v_2) + \nu v_1}{u - v_1} + h_1 - h_2, & k_2 > k_2^{(c)}. \end{cases} \quad (61)$$

As always, a special role is played by the value of the momenta where the excitation spectra equal zero. We term these the Fermi momenta k_i^f . When $\alpha \leq 0$, the Fermi momenta are

$$k_1^f = \frac{h_1}{v_1}, \quad k_2^f = \frac{h_2}{v_2}. \quad (62)$$

It can be verified that as long as $\alpha < 0$,

$$k_i^c > k_i^f, \quad (63)$$

and that $k_i^c = k_i^f$ if $\alpha = 0$. The excitation spectra for both species of chiral fermions are shown in Fig. 1.

The ground state densities can also be found from the $T \rightarrow 0$ limit of Eq. (55),

$$\rho_1(k_1) = \begin{cases} \frac{1}{2\pi}, & k_1 < k_1^f, \\ 0, & k_1 > k_1^f, \end{cases} \quad (64)$$

$$\rho_2(k_2) = \begin{cases} \frac{1}{2\pi}, & k_2 < k_2^f, \\ 0, & k_2 > k_2^f. \end{cases} \quad (65)$$

Let us examine $\epsilon_1(k_1)$ first. We see that in the region $k_1 \leq k_1^{(c)}$, these fermions behave as though they were non-interacting, since their spectrum corresponds to that of non-interacting chiral fermions dispersing with velocity v_1 . Beyond this range of momenta, the behavior of the fermions changes as the interaction forces them to disperse with a different velocity. Importantly, the Fermi momentum i.e., where $\epsilon_1(k_1) = 0$ matches the Fermi momentum of a non-interacting system of chiral fermions. Since the behavior of $\epsilon_1(k_1)$ changes at a momentum larger than k_1^f , the ground state of the v_1 fermions corresponds to a filled Fermi sea of non-interacting chiral

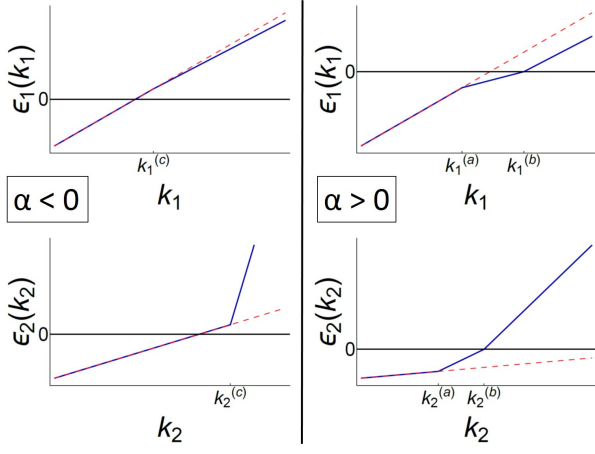


FIG. 1. Excitation spectra for case A1, where the parameters are taken, for the purpose of illustration, as $u = 6, v_1 = 4, v_2 = 1, h_1 = 9, h_2 = 2$. The figures in the left panel correspond to $\alpha < 0$ ($\nu = -20$), in which case both species of fermions remain non-interacting throughout the Fermi sea. The figures in the right panel correspond to $\alpha > 0$ ($\nu = 20$), and in this case the fermions interact within a finite range of momenta $k_i^{(a)} \leq k_i \leq k_i^{(b)}$. The red dashed lines in either case are the non-interacting excitation spectra, $k_i v_i - h_i$.

fermions, reflected in the ground state density $\rho_1(k_1)$, which equals $1/(2\pi)$, the momentum density for non-interacting free fermions.

Similarly, we observe that the spectrum of the v_2 fermions corresponds to that of non-interacting chiral fermions, since $\epsilon_2(k_2) = k_2 v_2 - h_2$ in the momentum range $k_2 \leq k_2^{(c)}$. The ground state of these fermions is thus also described by a filled Fermi sea of non-interacting fermions, with the Fermi momentum k_2^f and ground state density $\rho_2(k_2)$ also reflecting the non-interacting behavior.

We now consider the regime where $\alpha > 0$. Here, we again find that the spectra are piece-wise linear functions

$$\epsilon_1(k_1) = \begin{cases} k_1 v_1 - h_1, & k_1 < k_1^{(a)}, \\ \frac{k_1 u (v_1 - v_2) - \nu v_2}{2(u - v_2)} - \frac{h_1 + h_2}{2}, & k_1^{(a)} < k_1 < k_1^{(b)}, \\ \frac{k_1 u (v_1 - v_2) - \nu v_2}{(u - v_2)} - h_1 - h_2, & k_1 > k_1^{(b)} \end{cases} \quad (66)$$

$$\epsilon_2(k_2) = \begin{cases} k_2 v_2 - h_2, & k_2 < k_2^{(a)}, \\ \frac{k_2 (u (v_1 + v_2) - 2v_1 v_2) + \nu v_1}{2(u - v_1)} + \frac{h_1 - h_2}{2}, & k_2^{(a)} < k_2 < k_2^{(b)}, \\ \frac{k_2 (u (v_1 + v_2) - 2v_1 v_2) + \nu v_1}{u - v_1} + h_1 - h_2, & k_2 > k_2^{(b)}, \end{cases} \quad (67)$$

with the ground state densities given by

$$\rho_1(k_1) = \begin{cases} \frac{1}{2\pi}, & k_1 < k_1^{(a)} \\ \frac{1}{4\pi} \left(1 - \frac{u - v_1}{u - v_2} \right), & k_1^{(a)} < k_1 < k_1^{(b)}, \\ 0, & k_1 > k_1^{(b)}, \end{cases} \quad (68)$$

$$\rho_2(k_2) = \begin{cases} \frac{1}{2\pi}, & k_2 < k_2^{(a)}, \\ \frac{1}{4\pi} \left(1 + \frac{u - v_2}{u - v_1} \right), & k_2^{(a)} < k_2 < k_2^{(b)}, \\ 0, & k_2 > k_2^{(b)}. \end{cases} \quad (69)$$

Furthermore, the Fermi momenta, defined by $\epsilon_i(k_i^f) = 0$, are now

$$k_i^f = k_i^{(b)} \quad (70)$$

as can be easily verified.

We now contrast the behavior of $\epsilon_1(k_1)$ in this regime with that in the previous case. For $\alpha > 0$, as depicted in Fig. 1, we see that while the system displays non-interacting behavior deep within the Fermi sea i.e., for $k_1 \leq k_1^{(a)}$, this behavior changes before the spectrum crosses zero energy. In this case, the spectrum of the v_1 fermions deviates from the non-interacting spectrum in the vicinity of the Fermi momentum. Importantly, the ground state density $\rho_1(k_1)$ is also modified from the non-interacting value $1/(2\pi)$ in the vicinity of the Fermi momentum k_1^f but retains the non-interacting value for $k_1 \leq k_1^{(a)}$. Hence, the ground state of the system is described by a filled Fermi sea of chiral fermions that, at large negative momenta, behave as non-interacting chiral fermions, but interact close to the Fermi momentum with a modified momentum density and dispersion due to the weak resonant interactions.

Analogous behavior occurs for the v_2 particles when $\alpha > 0$, since their spectrum matches that of a non-interacting spectrum for $k_2 \leq k_2^{(a)}$ but the dispersion changes in the vicinity of the Fermi momentum k_2^f . The ground state density in the vicinity of the Fermi level also deviates from its non-interacting value.

Thus, we have explicitly found the excitation spectrum and the ground state densities for the system. The fact that the ground state properties of these chiral fermions are significantly modified depending on the parameter α is an indication that the system undergoes a quantum phase transition. For $\alpha \leq 0$, the ground state of the system behaves as though it is insensitive to interactions, reflected in the densities ρ_1, ρ_2 which remain $1/(2\pi)$, their value for free fermions, all through the Fermi sea. However, for $\alpha > 0$, the solution to our problem changes qualitatively since the particles now interact within a finite range of momenta in the vicinity of k_i^f , changing the ground state densities in this region.

We can further elucidate the nature of this change if we calculate the particle densities D_1, D_2 as functions of

the chemical potentials h_1, h_2 . We can then invert this relation to find the chemical potentials as functions of particle density, i.e., $h_i(D_1, D_2)$ and look for discontinuities in these functions or their derivatives.

The particle densities are defined as

$$D_1 = \int_{-\Lambda}^{\infty} dk_1 \rho_1(k_1) - D_1^{(0)}, \quad D_2 = \int_{-\Lambda}^{\infty} dk_2 \rho_2(k_2) - D_2^{(0)}. \quad (71)$$

Here, $D_i^{(0)}$ are the densities calculated at some reference point to cancel the contribution from the cut-off, Λ . We can also get the total energy density of the system,

$$\mathcal{E} = v_1 \int_{-\Lambda}^{\infty} dk_1 k_1 \rho_1(k_1) + v_2 \int_{-\Lambda}^{\infty} dk_2 k_2 \rho_2(k_2) - \mathcal{E}_1^{(0)} - \mathcal{E}_2^{(0)}, \quad (72)$$

and define the inverse compressibility as

$$\kappa_{ij}^{-1} = \frac{\partial^2 \mathcal{E}}{\partial D_i \partial D_j} = \frac{\partial h_i}{\partial D_j}, \quad i, j = 1, 2 \quad (73)$$

which satisfies $\kappa_{ij}^{-1} = \kappa_{ji}^{-1}$.

Let us consider the case $\alpha \leq 0$ first. Here, we find that,

$$D_1 = \frac{h_1}{2\pi v_1}, \quad D_2 = \frac{h_2}{2\pi v_2}, \quad (74)$$

which when inverted leads to

$$h_1(D_1, D_2) = 2\pi v_1 D_1, \quad h_2(D_1, D_2) = 2\pi v_2 D_2. \quad (75)$$

Thus, we find the inverse compressibility

$$\kappa^{-1} = \begin{pmatrix} 2\pi v_1 & 0 \\ 0 & 2\pi v_2 \end{pmatrix}, \quad (76)$$

which corresponds to the compressibility of a system of two independent species of non-interacting chiral fermions.

Next we consider the regime where $\alpha > 0$. Here, we find the chemical potentials

$$h_1 = \frac{2\pi D_1 (u^2 - v_1 v_2) + (u - v_1) (2\pi D_2 (u - v_2) + \nu)}{2u - v_1 - v_2},$$

$$h_2 = \frac{2\pi D_2 (u^2 - v_1 v_2) + (u - v_2) (2\pi D_1 (u - v_1) + \nu)}{2u - v_1 - v_2}, \quad (77)$$

from which we find the inverse compressibility

$$\kappa^{-1} = \frac{2\pi}{2u - v_1 - v_2} \begin{pmatrix} u^2 - v_1 v_2 & (u - v_1)(u - v_2) \\ (u - v_1)(u - v_2) & u^2 - v_1 v_2 \end{pmatrix}, \quad (78)$$

which distinctly differs from the compressibility in the regime $\alpha \geq 0$. Thus, even though the spectra remain gapless for all values of α , the compressibilities κ_{11} and κ_{22} are discontinuous, which indicates a phase transition. Since we now have the chemical potentials as functions of the particle densities, we can now also define a parameter

$$\beta(D_1, D_2) = 2\pi D_1 (u - v_1) + 2\pi D_2 (u - v_2) + \nu, \quad (79)$$

such that $\text{sgn}(\alpha(h_1, h_2)) = \text{sgn}(\beta(D_1, D_2))$. For fixed particle densities, as we vary the detuning ν , the discontinuity hence occurs at $\nu = -2\pi D_1 (u - v_1) - 2\pi D_2 (u - v_2)$.

We have thus shown that the Q3WI model in the weakly interacting regime undergoes a phase transition as a function of the particle densities of two species of particles at the point where $\alpha = \beta = 0$. The nature of this phase transition is such that the system goes from being completely non-interacting throughout the Fermi sea ($\beta \leq 0$) to being interacting within a finite range of momenta close to the Fermi momenta ($\beta > 0$). Since the compressibility is sensitive primarily to the ground state density in the vicinity of the Fermi level k_i^f and since the system's behavior near k_i^f changes abruptly as a function of β , it is intuitively clear that this change should manifest itself as a discontinuity in κ .

Although we have focused on a particular case here ($u > v_1 > v_2 > 0$), we find similar phenomena in all other cases as long as $u > v_1 > v_2$ or $v_1 > v_2 > u$ (with the cases where $v_2 > v_1$ understood by exchanging the v_1 and v_2 fermions). Specifically, in each case we find that the spectra remain gapless while the compressibilities κ display a discontinuity as a function of the parameter α in response to the change in the system's behavior close to the Fermi level. While the discussion of the ground state properties and associated phase transitions for all other cases is left to App. D, we now review those cases where the Q3WI model displays rather unconventional behavior.

We also note that while we will only plot the excitation spectra in what follows, the ground state densities may be simply inferred from these, since $\rho_i(k_i)$ equals $1/(2\pi)$ over the momentum range where $\epsilon_i(k_i)$ coincides with its non-interacting value. Conversely, if the spectrum deviates from $k_i v_i - h_i$ over some range of momenta within the Fermi sea, then the corresponding ground state density no longer equals $1/(2\pi)$ and the v_i fermions are hence interacting over this range. By definition, $\rho_i(k_i)$ vanishes for $k_i > k_i^f$.

Interacting behavior deep within the Fermi sea

In the case considered above, regardless of $\text{sgn}(\alpha)$, both species of chiral fermions displayed non-interacting behavior at large negative momenta, i.e., deep within the Fermi sea. This is in accordance with expectations, since interactions typically only modify the behavior in the vicinity of the Fermi momenta. However, if we change the velocities such that $u > v_1 > 0 > v_2$ with $u(v_1 + v_2) - 2v_1 v_2 < 0$, i.e., case A2i of our classification, we encounter unusual behavior in the spectrum of both species of fermions, as illustrated in Fig. 2.

Specifically, regardless of $\text{sgn}(\alpha)$ we find that both species of fermions remain interacting deep into the Fermi sea since their ground state densities deviate from $1/(2\pi)$ (see App. D 1a for details). For $\alpha < 0$, we find that the v_1 particles display interacting behavior for large neg-

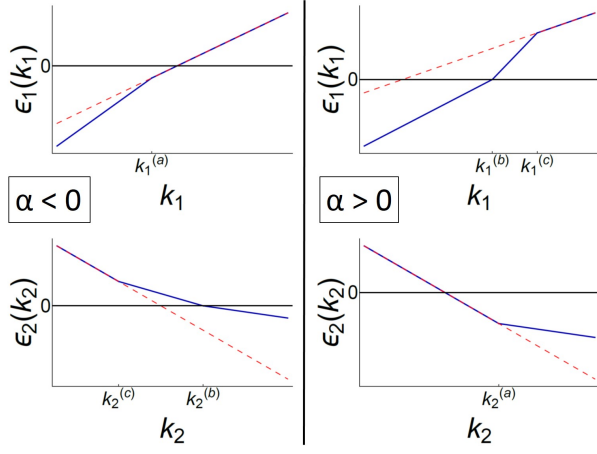


FIG. 2. Excitation spectra for case A2i, with $u = 10, v_1 = 2, v_2 = -10, h_1 = 2, h_2 = 3$. The left-hand panel depicts the regime $\alpha < 0$ ($\nu = 20$), where the v_2 fermions interact throughout the Fermi sea while the v_1 species interacts deep within the Fermi sea but becomes non-interacting for $k_1^{(a)} \leq k_1 \leq k_1^f$. The right-hand panel depicts the case $\alpha > 0$ ($\nu = -30$), where the behavior is reversed. The red dashed lines are the spectra in the non-interacting case.

ative momenta while remaining non-interacting in the vicinity of k_1^f whereas the v_2 particles interact for all momenta $k_2 \geq k_2^f$ (since $v_2 < 0$ here, we impose a positive momentum cut-off on these fermions). That the ground state densities are modified from $1/(2\pi)$ is reflected in the deviation of the fermionic spectra from the non-interacting dispersions. In addition, we find that the densities change at precisely those momenta at which the dispersions change. When $\alpha > 0$, the behavior of the v_1 and v_2 fermions is reversed since now the v_1 particles interact for all $k_1 \leq k_1^f$ while the v_2 fermions behave as non-interacting fermions in a finite range of momenta close to k_2^f .

The change in behavior is reflected in the compressibilities, which are discontinuous at $\alpha = 0$. For instance, we find that $\kappa_{11}^{-1} = 2\pi v_1$ for $\alpha < 0$, which is the compressibility associated with non-interacting chiral fermions dispersing with velocity v_1 . However, for $\alpha > 0$, κ_{11}^{-1} changes its value since now these fermions are interacting throughout the Fermi sea. Similar behavior is displayed by the v_2 fermions. Thus, in this parameter regime we find that the Q3WI model displays behavior starkly in contrast with that expected from weakly interacting fermions, since in our model the chiral fermions remain interacting far into the Fermi sea.

Interaction induced loss of chirality

Thus far, both cases encountered have the property that the fermionic spectra remain gapless, and though the velocities with which they disperse change abruptly at certain special momenta, the chirality of each species

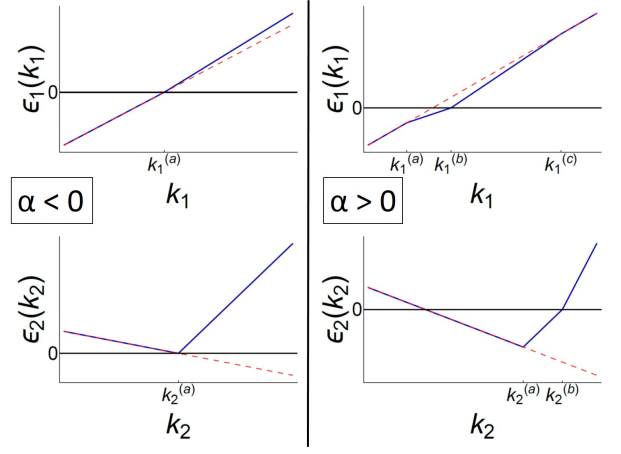


FIG. 3. Excitation spectra for case A2ii, with $u = 6, v_1 = 4, v_2 = -3, h_1 = 2, h_2 = 3$. The plots on the left are for $\nu = 8$, corresponding to $\alpha = 0$, while the ones on the right are for $\nu = -10$ corresponding to $\alpha > 0$. The red dashed lines are the excitation spectra for a non-interacting system ($g = 0$).

stays invariant throughout the Fermi sea and matches that of the non-interacting case i.e., $\text{sgn}(\epsilon'_i(k_i)) = \text{sgn}(v_i)$. If we instead consider the parameter regime where $u > v_1 > 0 > v_2$ with $u(v_1 + v_2) - 2v_1v_2 > 0$ i.e., case A2ii, then this is no longer the case.

For velocities that satisfy the above conditions, we find that the parameter β is simply given by the density of the v_2 fermions, $\beta = D_2$ (see App. D 1 b for details). Hence, the case $\beta < 0$ (equivalently $\alpha < 0$) is un-physical here and we must instead consider how the system changes when β becomes non-zero. Since $\beta = 0$ corresponds to a vanishing density of the v_2 particles, we expect that $\kappa_{22}^{-1} = 0$ and that κ_{11}^{-1} corresponds to the compressibility of non-interacting chiral fermions, $2\pi v_1$. Indeed, as shown in Fig. 3, $\epsilon_1(k_1)$ coincides with the non-interacting spectrum throughout the Fermi sea and $\rho_1(k_1) = 1/(2\pi)$ in this region. Since $\epsilon_2(k_2) > 0$ for all k_2 , this implies a vanishing momentum density of the v_2 particles, consistent with $D_2 = 0$.

However, as soon as we have a non-zero density D_2 , the behavior changes drastically. In particular, we see from Fig. 3 that the v_1 particles begin interacting close to the Fermi momentum $k_1^f = k_1^{(b)}$. This change is also reflected in κ_{11} . More interestingly, we see that the spectrum $\epsilon_2(k_2)$ is no longer chiral and crosses zero energy at two distinct Fermi momenta. The chirality of these fermions changes sign abruptly at $k_2^{(a)}$ and they display non-interacting behavior close to $k_2^{f,1} = h_2/v_2$ but interact in the vicinity of $k_2^{f,2} = k_2^{(b)}$, with the compressibility reflecting this behavior. Thus, we see that in a certain parameter regime, even weak interactions are sufficient to change the chiral nature of the v_2 particles. This is remarkable since, typically, we expect that in the absence of back-scattering the velocity should never change sign and yet, we find that this is indeed the behavior exhibited

by the Q3WI model in the weakly interacting regime.

In this section, we have developed a procedure for deriving the weakly interacting, zero temperature ground state densities and excitation spectra of the Q3WI model for case A. In particular, we have demonstrated the existence of a quantum phase transition in this model through an example, with the details of all other cases left to Appendix D. Furthermore, we have discussed the qualitatively different behaviors exhibited by this model, focusing on the unconventional nature of the spectra that arise as a consequence of weak interactions.

VII. QUASI-CONDENSATES AT WEAK INTERACTIONS (CASE B)

We now consider the case $v_1 > u > v_2$, where the Q3WI model exhibits qualitatively different behavior compared to that encountered in Sec. VI. While in the previous section we saw that the spectra were piece-wise linear functions of momentum and that the ground state densities were momentum-independent constants, here we find that the dispersions, while still remaining gapless, are no longer linear in momentum and that the densities $\rho_i(k_i)$ are momentum dependent.

The origin of this change in behavior lies in the fact that when the atomic velocities v_i bracket the molecular velocity u , the ground state densities diverge in the limit $g \rightarrow 0$. This is analogous to the behavior of the Lieb-Linger model [38, 39] in the weakly interacting limit. In our case, we will similarly find that it is insufficient to keep only the leading order g -independent δ -function term in the integral kernel $K(k_1, k_2)$ (45).

In order to show this explicitly, let us consider Eq. (48), where only the δ -function term in the $g \rightarrow 0$ approximation of the kernel (Eq. (45)) is kept in the reduced kernel \tilde{K} , given by Eq. (46). We also make the ansatz that the excitation spectrum $\epsilon_i(k_i)$ crosses zero energy only at a single Fermi point k_i^f . We will justify our ansatz later for the cases where $\text{sgn}(v_1) = \text{sgn}(v_2)$; we are unable to find a solution when $\text{sgn}(v_1) = -\text{sgn}(v_2)$ as this ansatz breaks down.

In the $T \rightarrow 0$ limit, the equations for the ground state densities thus become

$$\rho_1(k_1) = \frac{1}{2\pi} + \frac{v_1 - u}{2\pi} \int_{-\Lambda}^{k_2^f} dk_2 \rho_2(k_2) \tilde{K}(k_1, k_2), \quad (80)$$

$$\rho_2(k_2) = \frac{1}{2\pi} + \frac{u - v_2}{2\pi} \int_{-\Lambda}^{k_1^f} dk_1 \rho_1(k_1) \tilde{K}(k_1, k_2), \quad (81)$$

where \tilde{K} is the reduced integral kernel (46). Here, we have assumed without loss of generality that $v_1, v_2 > 0$ since the case where $v_1, v_2 < 0$ follows similarly. With the kernel \tilde{K} being a δ -function, the integral in the right hand side of Eq. (80) is non-zero only if

$$\frac{-\Lambda(u - v_2) + \nu}{v_1 - u} \leq k_1 \leq \frac{k_2^f(u - v_2) + \nu}{v_1 - u}, \quad (82)$$

while the integral in the right hand side of Eq. (81) is non-zero only if

$$\frac{-\Lambda(v_1 - u) - \nu}{u - v_2} \leq k_2 \leq \frac{k_1^f(v_1 - u) - \nu}{u - v_2}. \quad (83)$$

For k_i that satisfy these conditions, Eq. (80) becomes

$$\begin{aligned} \rho_1(k_1) &= \frac{1}{2\pi} + \frac{v_1 - u}{u - v_2} \rho_2 \left(\frac{k_1(v_1 - u) - \nu}{u - v_2} \right), \\ \rho_2(k_2) &= \frac{1}{2\pi} + \frac{u - v_2}{v_1 - u} \rho_1 \left(\frac{k_2(u - v_2) + \nu}{v_1 - u} \right). \end{aligned} \quad (84)$$

These are a simple set of algebraic equations that lead to

$$\rho_1(k_1) = \frac{1}{2\pi} \left(1 - \frac{u - v_1}{u - v_2} \right) + \rho_1(k_1). \quad (85)$$

This equation has no solutions and hence clearly demonstrates that keeping only the reduced kernel \tilde{K} is insufficient. We are thus forced to keep the $O(g^2)$ term in the kernel (45) in order to establish the leading order behavior of the ground state densities in this regime.

Owing to this, the procedure for finding the zero temperature behavior is different from that employed in the previous section VI, where we first found the finite temperature solution and then took the limit $T \rightarrow 0$. Here, we work directly at zero temperature. However, in order to find an analytically tractable solution, we make an ansatz that there is only a single Fermi momentum k_i^f for the fermionic species i , which allows us to derive the ground state densities as a function of k_i^f . Given $\rho_i(k_i)$, we then calculate the particle densities D_i and the total energy density \mathcal{E} in terms of k_i^f . From these expressions, we then extract the chemical potential $h_i = \partial\mathcal{E}/\partial D_i$ and the inverse compressibility $\kappa_{ij}^{-1} = \partial h_i / \partial D_j$ to leading order in the coupling strength g .

We note that while our results for physical quantities, such as the total energy, depend on the cut-off Λ , the compressibilities κ_{ij} become cut-off independent in the limit $\Lambda \rightarrow \infty$. We also note that since we are unable to find an analytic solution when $v_1 > 0 > v_2$, we will briefly discuss the failure of our ansatz in this region of parameter space at the end of this section.

We now study the case $v_1 > u > v_2 > 0$ in detail and demonstrate the presence of a quasi-condensate phase and a quantum phase transition within this regime. Following the discussion above, we see that in order to find an analytic solution for the ground state densities in the weakly interacting limit, we are forced to keep the $O(g^2)$ term in the asymptotic expansion of the integral kernel $K(k_1, k_2)$. Thus, the TBA equations in the zero temperature limit are given by

$$\begin{aligned} \rho_1(k_1) &= \frac{1}{2\pi} + \frac{v_1 - u}{2\pi} \int_{-\Lambda}^{k_2^f} dk_2 \rho_2(k_2) K(k_1, k_2), \\ \rho_2(k_2) &= \frac{1}{2\pi} + \frac{u - v_2}{2\pi} \int_{-\Lambda}^{k_1^f} dk_1 \rho_1(k_1) K(k_1, k_2), \end{aligned} \quad (86)$$

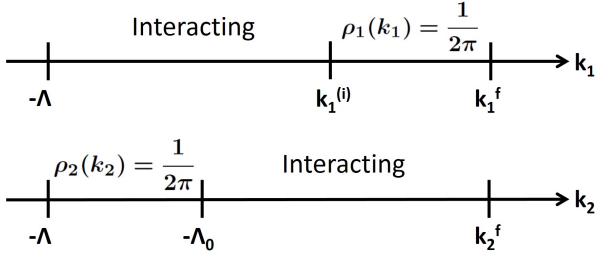


FIG. 4. For the case where $v_1 - u < u - v_2$ and $\alpha < 0$, the interactions are restricted to lie between certain ranges of momenta, shown above. Outside these regions, the densities $\sim 1/(2\pi)$.

where K is now given by Eq. (45). For momenta larger than the Fermi momentum, $k_i > k_i^f$, the densities vanish i.e., $\rho_i(k_i > k_i^f) = 0$.

The leading order term in the kernel $K(k_1, k_2)$ is still a δ -function, which only acts (gives a non-zero contribution to the integrals above) if the momenta are in the range

$$\frac{-\Lambda(u - v_2) + \nu}{v_1 - u} < k_1 < k_1^{(i)}, \quad (87)$$

for the first equation in Eq. (86) and if

$$\frac{-\Lambda(v_1 - u) - \nu}{u - v_2} < k_2 < k_2^{(i)}, \quad (88)$$

for the second equation in Eq. (86), where we have defined

$$k_1^{(i)} = \frac{k_2^f(u - v_2) + \nu}{v_1 - u}, \quad k_2^{(i)} = \frac{k_1^f(v_1 - u) - \nu}{u - v_2}. \quad (89)$$

For momenta outside this range (but within the Fermi sea), the δ -function does not act and so the ground state densities are trivially given as

$$\rho_1(k_1) = \frac{1}{2\pi} + O(g^2), \quad \rho_2(k_2) = \frac{1}{2\pi} + O(g^2), \quad (90)$$

since the next term in $K(k_1, k_2) \propto g^2$.

In the following discussion, we assume without loss of generality that $v_1 - u < u - v_2$, since we find that the compressibilities are independent of this choice in the limit

$\Lambda \rightarrow \infty$. In this case, Eqs. (87) and (88), which specify the range of momenta for which the δ -function term in the kernel $K(k_1, k_2)$ contributes non-trivially to Eq. (86), can be replaced by

$$\begin{aligned} -\Lambda < k_1 < k_1^{(i)}, \\ -\Lambda_0 < k_2 < k_2^{(i)}, \end{aligned} \quad (91)$$

where

$$\Lambda_0 = \frac{\Lambda(v_1 - u) + \nu}{u - v_2}. \quad (92)$$

Thus, the particles of the first species will interact for all momenta up to the cut-off while the particles of the second species will become non-interacting for large negative momenta $-\Lambda < k_2 < -\Lambda_0$.

It is now convenient to introduce the parameter

$$\alpha(k_1^f, k_2^f, \nu) = k_1^f(u - v_1) + k_2^f(u - v_2) + \nu, \quad (93)$$

which also controls the range over which the particles interact. If we consider $\alpha < 0$, then the particles of the first species remain interacting only up to $k_1 = k_1^{(i)}$, while the particles of the second species interact all the way up to k_2^f . On the other hand, if $\alpha > 0$, then the first species of particles interact up to k_1^f while the second species of particles only interact up to $k_2^{(i)}$. This is shown schematically for $\alpha < 0$ in Fig. 4.

We now elucidate the steps required to find the leading order solution for the ground state densities in the case where $\alpha < 0$, with the solutions for $\alpha = 0$ and $\alpha > 0$ obtained by following the same procedure. As shown in Fig. 4, for momenta outside the interacting region i.e., where the δ -function in the kernel does not act, the densities to leading order in g are

$$\begin{aligned} \rho_1(k_1) &= \frac{1}{2\pi}, & k_1^{(i)} < k_1 < k_1^f, \\ \rho_2(k_2) &= \frac{1}{2\pi}, & -\Lambda < k_2 < -\Lambda_0. \end{aligned} \quad (94)$$

For momenta k_i in the range set by Eq. (91), however, the momentum densities satisfy

$$\begin{aligned} \rho_1(k_1) &= \frac{1}{2\pi} - \frac{u - v_1}{u - v_2} \rho_2 \left(-\frac{k_1(u - v_1) + \nu}{u - v_2} \right) - g^2 \frac{u - v_1}{2\pi(v_1 - v_2)} \int_{-\Lambda}^{k_2^f} dk_2 \frac{\rho_2(k_2)}{(k_1(u - v_1) + k_2(u - v_2) + \nu)^2}, \\ \rho_2(k_2) &= \frac{1}{2\pi} - \frac{u - v_2}{u - v_1} \rho_1 \left(-\frac{k_2(u - v_2) + \nu}{u - v_1} \right) + g^2 \frac{u - v_2}{2\pi(v_1 - v_2)} \int_{-\Lambda}^{k_1^f} dk_1 \frac{\rho_1(k_1)}{(k_1(u - v_1) + k_2(u - v_2) + \nu)^2}. \end{aligned} \quad (95)$$

In order to solve these equations, we break the integrals

into the interacting and non-interacting regions, and re-

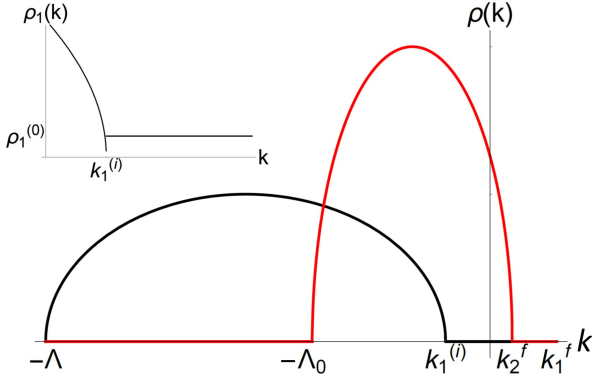


FIG. 5. The analytic solution for the ground state densities, $\rho_1(k_1)$ (in black) and $\rho_2(k_2)$ (in red) are plotted. Here $g = 0.1$, $v_1 = 5$, $u = 4$, $v_2 = 2$, $\nu = -20$, $\Lambda = 100$, $k_1^f = 15$, and $k_2^f = 5$. These are shown for the case where $\alpha < 0$. The in-set shows $\rho_1(k_1)$ in the vicinity of $k_1^{(i)}$, where its behavior changes from interacting to non-interacting, with $\rho_1^{(0)} = 1/(2\pi)$ the non-interacting value. The discontinuity seen here is an artefact of the small g approximation.

place $\rho_i(k_i)$ by its non-interacting value $1/(2\pi)$ in the latter.

As discussed before, we are keeping the $O(g^2)$ term in the integral kernel K . Keeping only the leading order $\sim 1/g^2$ terms, we find an integral equation for $\rho_1(k_1)$

$$\int_{-\Lambda}^{k_1^{(i)}} dk' \frac{\rho_1(k')}{(k' - k)^2} = \frac{(v_1 - v_2)(u - v_1)}{2g^2} \left(1 - \frac{u - v_1}{u - v_2} \right), \quad (96)$$

the solution to which is (see App. E)

$$\rho_1(k_1) = \frac{1}{2\pi g^2} \frac{(v_1 - u)(v_1 - v_2)^2}{u - v_2} \sqrt{(k_1 + \Lambda)(k_1^{(i)} - k_1)}, \quad (97)$$

for $-\Lambda < k_1 < k_1^{(i)}$. Similarly, we find that

$$\rho_2(k_2) = \frac{1}{2\pi g^2} \frac{(u - v_2)(v_1 - v_2)^2}{|u - v_1|} \sqrt{(k_2^f - k_2)(k_2 + \Lambda_0)}, \quad (98)$$

for $-\Lambda_0 < k_2 < k_2^f$. Thus, we find qualitatively different behavior in this parameter regime, since unlike the densities found in Sec. VI, which were discontinuous momentum-independent constants, the ground state densities found here are momentum dependent and diverge in the limit $g \rightarrow 0$. Note the striking resemblance of this solution to the behavior of the weakly interacting Bose gas (Lieb-Liniger model [38]). Hence the conclusion that the weakly interacting regime of the Q3WI with velocities such that $v_1 > u > v_2 > 0$ describes what we term a quasi-condensate phase.

These ground state densities $\rho_i(k_i)$ are illustrated in Fig. 5. In order to verify that our solution indeed satisfies the TBA equations, we numerically substitute our solution into the integral equations (86) but now with the complete integral kernel Eq. (20) and match the left

and right hand sides of those equations. We find excellent agreement between the two for $g \ll 1$, hence validating our analytic solution.

It is important to note that our solution, given in Eqs. (97) and (98), breaks down at the end points, as it predicts that the densities vanish there as an artefact of the small g approximation, whereas in reality the densities smoothly connect with the $1/(2\pi)$ densities of the non-interacting regions given by Eq. (94).

Due to this, unlike in Sec. VI where we could find an expression for the excitation spectra ϵ_i and demand that they vanish at the Fermi-momenta in order to find the chemical potentials h_i , here our expressions for ϵ_i —obtained by solving integral equations similar to those for the densities—will always vanish at the end points for any h_i . Thus, in a way which parallels the case of the weakly interacting Lieb-Liniger gas, we cannot obtain h_i by finding the excitation spectra but must use the method described at the beginning of this section, wherein we must find the particle densities D_i and total energy density \mathcal{E} as functions of the Fermi momenta k_i^f in order to derive the chemical potentials and inverse compressibility.

To implement this method, we compute the particle densities

$$D_1 = \int_{-\Lambda}^{k_1^f} dk_1 \rho_1(k_1), \quad D_2 = \int_{-\Lambda}^{k_2^f} dk_2 \rho_2(k_2), \quad (99)$$

where the densities ρ_i are given by Eqs. (94), (97), and (98). These integrals can be evaluated analytically in order to find the particle densities as functions of the Fermi momenta, i.e. $D_i = D_i(k_1^f, k_2^f)$. Similarly, we can express the total energy

$$\mathcal{E} = v_1 \int_{-\Lambda}^{k_1^f} dk_1 k_1 \rho_1(k_1) + v_2 \int_{-\Lambda}^{k_2^f} dk_2 k_2 \rho_2(k_2) \quad (100)$$

as a function of the Fermi momenta, $\mathcal{E} = \mathcal{E}(k_1^f, k_2^f)$. The chemical potentials are then found from the derivatives

$$h_i = \frac{\partial \mathcal{E}}{\partial D_i} = \sum_{n=1,2} \frac{\partial k_n^f}{\partial D_i} \frac{\partial \mathcal{E}}{\partial k_n^f}. \quad (101)$$

Differentiating once more allows us to find the inverse compressibilities. Importantly, we take the limit $\Lambda \rightarrow \infty$ in order to find the leading order (in g) compressibilities, which are cut-off independent,

$$\begin{aligned} [\kappa]_{ij}^{-1} &= \lim_{\Lambda \rightarrow \infty} \frac{\partial^2 \mathcal{E}}{\partial D_i \partial D_j} \\ &= \lim_{\Lambda \rightarrow \infty} \sum_{m,n=1,2} \frac{\partial k_m^f}{\partial D_i} \frac{\partial}{\partial k_m^f} \left(\frac{\partial k_n^f}{\partial D_j} \frac{\partial \mathcal{E}}{\partial k_n^f} \right) \end{aligned} \quad (102)$$

Before we proceed with the calculation, we must justify our ansatz that the excitation spectra cross zero-energy only once. In order to do this, we must check that the excitation energies remain negative for all $k_i \leq k_i^f$ since by

definition, $\epsilon_i(k_i) < 0$ when $\rho_i(k_i) > 0$. This will demonstrate that our solutions are consistent with our initial assumption that $\epsilon_i(k_i) = 0$ only at a single point.

To find the excitation spectra at zero temperature in the weakly interacting limit, we must solve the coupled integral equations

$$\begin{aligned}\epsilon_1(k_1) &= k_1 v_1 - h_1 + \frac{u - v_2}{2\pi} \int_{-\Lambda}^{k_2^f} dk_2 K(k_1, k_2) \epsilon_2(k_2), \\ \epsilon_2(k_2) &= k_2 v_2 - h_2 - \frac{u - v_1}{2\pi} \int_{-\Lambda}^{k_1^f} dk_1 K(k_1, k_2) \epsilon_1(k_1),\end{aligned}\quad (103)$$

with the kernel given by Eq. (45).

The solution proceeds in a manner similar to that for the densities, as in the range of momenta where the δ -function does not act, we find that (for $\alpha < 0$)

$$\begin{aligned}\epsilon_1(k_1) &= k_1 v_1 - h_1, \quad k_1^{(i)} < k_1 < k_1^f, \\ \epsilon_2(k_2) &= k_2 v_2 - h_2, \quad -\Lambda < k_2 < -\Lambda_0.\end{aligned}\quad (104)$$

On the other hand, for the excitation spectra in the interacting region, we must solve integral equations following from Eqs. (103), similarly to how it was done for the densities. We find that the leading order $\sim 1/g^2$ solutions for these are

$$\begin{aligned}\epsilon_1(k_1) &= \frac{(v_1 - u)(v_1 - v_2)}{g^2} \sqrt{(k_1^{(i)} - k_1)(k_1 + \Lambda)} \\ &\times \left(u \frac{v_1 - v_2}{u - v_2} \left(\frac{k_1^{(i)} - \Lambda + 2k_1}{4} \right) - h_1 - h_2 - \frac{\nu v_2}{u - v_2} \right),\end{aligned}\quad (105)$$

for $-\Lambda < k_1 < k_1^{(i)}$, and

$$\begin{aligned}\epsilon_2(k_2) &= \frac{(u - v_2)(v_1 - v_2)}{g^2} \sqrt{(k_2^f - k_2)(k_2 + \Lambda_0)} \\ &\times \left(u \frac{v_1 - v_2}{v_1 - u} \left(\frac{k_2^f - \Lambda_0 + 2k_2}{4} \right) - h_1 - h_2 - \frac{\nu v_1}{v_1 - u} \right),\end{aligned}\quad (106)$$

for $-\Lambda_0 < k_2 < k_2^f$. While we found these solutions for arbitrary h_i , in practice those must be fixed according to Eq. (101).

For the case $\alpha < 0$, with the chemical potentials appropriately fixed, the excitation spectra are plotted in Fig. 6.

Although we have only stated solutions for $k_i < k_i^f$ here, the integral equations (103) can also be solved for momenta larger than the Fermi momenta i.e., $k_i > k_i^f$. We have verified that indeed $\epsilon_i(k_i > k_i^f) > 0$, hence vindicating our ansatz that the spectra only cross zero energy at a single point.

Now that we have constructed the solution to our problem, we would like to proceed with calculating the compressibilities to verify that they change when α changes

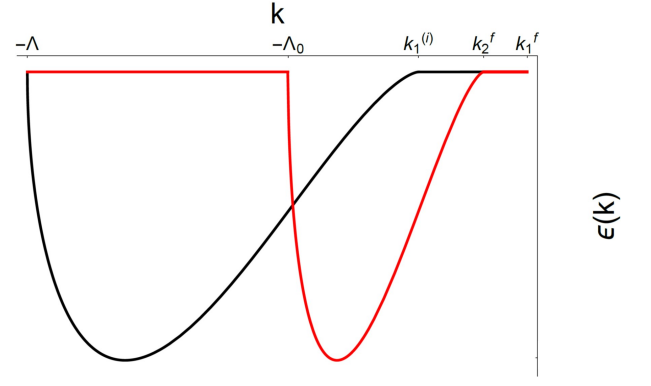


FIG. 6. The analytic solution for the excitation energies, $\epsilon_1(k_1)$ (in black) and $\epsilon_2(k_2)$ (in red) are plotted. Here $g = 0.1$, $v_1 = 5$, $u = 4$, $v_2 = 2$, $\nu = -20$, $\Lambda = 100$, $k_1^f = 15$, and $k_2^f = 5$. This is for the case where $\alpha < 0$. For $k_i > k_i^f$, the excitation spectra $\epsilon_i(k_i) > 0$, hence confirming our ansatz that the spectra only cross zero energy once.

its sign, indicating a phase transition when $\alpha = 0$. At first glance, given that we have derived analytic expressions for the ground state densities, it appears straightforward to derive analytic expressions for the particle densities D_i (99) and the total energy \mathcal{E} (100) and to then evaluate the derivatives in Eq. (102) to determine compressibilities.

However, as discussed earlier, our expressions for the ground state densities ρ_i in the interacting regions, given by Eqs. (97), (98), break down in the vicinity of the end points i.e., momenta where the behavior changes from interacting to non-interacting. Since the true behaviour of the densities is expected to be one where they connect smoothly with the non-interacting value $1/(2\pi)$, we must account for the possibility that perturbative in g corrections to our solutions lead to non-trivial contributions to the compressibilities. Hence, care must be taken while evaluating the derivatives that appear in Eq. (102), a detailed discussion of which is presented in App. F.

The analysis presented in the Appendix shows that any corrections to our expressions for the ground state densities will in fact not contribute to the leading order (in g) ground state inverse compressibilities, which we find are

$$\begin{aligned}\kappa^{-1} &= 2\pi v_1 \begin{pmatrix} 1 & -1 \\ -1 & 1 \end{pmatrix}, \quad \alpha < 0, \\ \kappa^{-1} &= 2\pi v_2 \begin{pmatrix} 1 & -1 \\ -1 & 1 \end{pmatrix}, \quad \alpha > 0.\end{aligned}\quad (107)$$

We first note that the cut-off, Λ , drops out entirely in these expressions since we are working in the limit $\Lambda \rightarrow \infty$. We also observe that since we are working in the regime where $v_1 > u > v_2 > 0$, the inverse compressibilities are well-defined and positive.

The situation is somewhat more involved for the compressibilities themselves. We observe that the inverse compressibility matrices in either regime are non-

invertible. This is another artifact of the small g approximation since it is possible to show (see App. F) that these matrices are necessarily invertible once corrections to the leading order solutions are accounted for. Thus, in principle it is possible to find the compressibility matrix κ by extending our analytic solutions for the densities ρ_i beyond leading order.

The inverse compressibility matrices (107) suffice, however, for the purposes of establishing a phase transition within the quasi-condensate regime since we see that κ^{-1} is discontinuous as a function α . In particular, κ^{-1} equals the non-interacting compressibility of the first fermionic species if $\alpha < 0$, and of the second fermionic species if $\alpha > 0$. This can be understood as follows: for $\alpha < 0$, the majority v_1 particles are non-interacting in the vicinity of their Fermi momentum k_1^f since $\rho_1(k_1) = 1/(2\pi)$ here. Since the compressibility depends primarily on the behavior close to the Fermi point, we expect it to take on its non-interacting value for the v_1 particles.

Thus, if $\alpha < 0$, only particles of the first species contribute to the compressibility of both species. The situation is reversed when $\alpha > 0$ since the compressibility is now determined by the second species of fermions, which are non-interacting in the vicinity of k_2^f .

Just as was done in the prior study of Case A in Sec. VI, we can re-express the parameter α in terms of the densities D_1 and D_2 , to get a clear criterion of the transition as a function of densities. It is straightforward to check by integrating (97) and (98) that the contribution of the interacting regions to D_1 is exactly equal to their contribution to D_2 , and hence

$$D_2 - D_1 = \frac{1}{2\pi} \left((\Lambda - \Lambda_0) - (k_1^f - k_1^{(i)}) \right). \quad (108)$$

In turn, we rewrite this with the help of Eq. (89) as

$$D_2 - D_1 = \frac{\alpha}{2\pi(v_1 - u)} + \frac{\Lambda - \Lambda_0}{2\pi}. \quad (109)$$

Therefore we see that since the transition happens when α changes sign, this is equivalent to saying that the transition happens when

$$\beta = D_2 - D_1 - (\Lambda - \Lambda_0)/(2\pi) \quad (110)$$

changes sign. Since the last term in Eq. (110) is a density independent constant, this gives a clear criterion for transition as a function of the densities.

When $v_1 > 0 > v_2$ (with $v_1 > u > v_2$) we are unable to find a consistent analytic solution for the ground state densities and excitation spectra. In particular, our ansatz that the excitation spectra cross zero energy at only one point breaks down since making that ansatz leads to negative compressibilities, indicating the instability of our solution. Additionally, if we construct the excitation spectrum for this case following our steps in the previous sections, we find that it is positive where the densities are positive: another contradiction, since by definition, $\epsilon(k) < 0$ where $\rho(k) > 0$. Thus, our ansatz

that there is only one Fermi-point breaks down here. This is similar to the case in Sec. D1b where the excitation spectrum changes sign twice. While we did find some numerical evidence for this being the case, our solution did not converge and we will hence leave this case for future work.

VIII. CONCLUSIONS

In this paper, we have studied a one-dimensional model of chiral fermions interacting through an s -wave Feshbach resonance. In particular, we have demonstrated that this model is host to a plethora of possible behaviors in the weakly interacting regime, from one where the fermions remain interacting deep within their Fermi seas to one where they become non-chiral. We also find that fermions interacting via a Feshbach resonance, in the limit of weak interactions, can exhibit behavior that closely resembles that of the weakly interacting Bose gas, a case that we have dubbed the “quasi-condensate” phase of our model.

While we have demonstrated the existence of a quantum phase transition through the discontinuity in the zero temperature compressibility, the precise nature of this transition remains unclear and may benefit from a bosonization study. It would also be interesting to further investigate the thermodynamic properties of the phases where the particles interact deep into the Fermi sea—is this unusual behavior reflected in any quantities besides the compressibility?

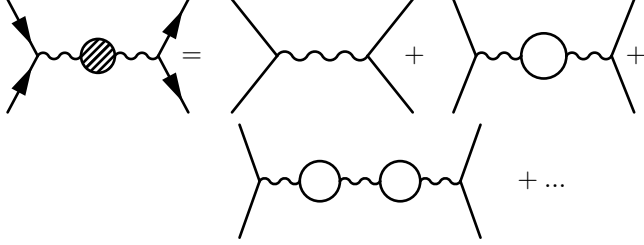
The full phase diagram of our system as a function of the interaction strength g and of the particle densities remains the subject of future work, since we can only probe the weak g and strong g limits analytically. Studying generic values of g would probably require a numerical study of the Bethe Ansatz equations derived here.

We were unable to find an analytic solution in one case, that when $v_1 > 0 > v_2$ and the molecular velocity u lies in between the atomic velocities v_i . In order to complete our characterization of this model, we must thus develop a numerical solution for the Q3WI model in this particular regime. However, from our analysis of the other cases, we expect that this particular regime should also host a quasi-condensate phase and exhibit a quantum phase transition as a function of particle densities.

Acknowledgements: We are grateful to Will Jay, Alex Kamenev, Sergej Moroz, and Yang-Zhi Chou for useful discussions. We acknowledge financial support from NSF grants DMR-1205303 and PHY-1211914.

Appendix A: T -Matrix calculation of scattering amplitudes

Here, we calculate the scattering amplitude of an a_1 particle and an a_2 particle governed by the Q3WI Hamiltonian Eq. (3). This is done by calculating the amplitude for the diagram



Since these diagrams form a geometric series, they can be re-summed exactly to give the T -matrix amplitude

$$T(k, E) = \frac{g^2}{D^{-1}(k, E) - g^2 \Pi(k, E)}, \quad (\text{A1})$$

where

$$\text{wavy line} = D(k, E),$$

$$\text{circle} = \Pi(k, E).$$

Here, D is the retarded Green's function for the b -particles

$$D(k, E) = \frac{1}{E - uk - \nu + i0}, \quad (\text{A2})$$

and Π is the polarization operator

$$\Pi = \int \frac{d\omega}{2\pi i} \frac{dk}{2\pi} G_{0,1} \left(\frac{p}{2} + k, E + \omega \right) G_{0,2} \left(\frac{p}{2} - k, -\omega \right), \quad (\text{A3})$$

where $G_{0,i}$ is the retarded Green's function for the a_i particles

$$G_{0,i}(k, E) = \frac{1}{E - v_i k + i0}, \quad (\text{A4})$$

and $p = k_1 + k_2$ is the centre of mass momentum. We find that

$$\begin{aligned} \Pi &= \int_{-\infty}^{\infty} \frac{dk}{2\pi} \frac{1}{E - \frac{p}{2}(v_1 + v_2) - k(v_1 - v_2) - i\epsilon}, \\ &= -\frac{i}{2(v_1 - v_2)}. \end{aligned} \quad (\text{A5})$$

Since the energy is given by $E = k_1 v_1 + k_2 v_2$, we find

$$T = \frac{g^2}{\frac{ig^2}{2(v_1 - v_2)} + k_1 v_1 + k_2 v_2 - u(k_1 + k_2) - \nu}. \quad (\text{A6})$$

To calculate the S -matrix from the T -matrix, we note that the scattering amplitude f equals $\frac{S-1}{2}$ and for a linear dispersion satisfies [32]

$$\begin{aligned} f(k_1, k_2) &= -i \frac{T(k_1, k_2)}{2(v_1 - v_2)}, \\ &= \frac{-ig^2}{ig^2 + 2(v_1 - v_2)(k_1(v_1 - u) + k_2(v_2 - u) - \nu)}. \end{aligned} \quad (\text{A7})$$

Appendix B: Linearisation of the continuum two-channel model

Here, we relate the scattering amplitude for the two-channel Hamiltonian Eq. (1), to that of the Q3WI Hamiltonian by linearising the two-channel model in the vicinity of certain Fermi points. We first calculate the T -matrix for Eq. (1), following the method outlined in App. A,

$$T = \frac{g^2}{\frac{ig^2 m_a}{k_1 - k_2} + \frac{k_1^2}{2m_a} + \frac{k_2^2}{2m_a} - \frac{(k_1 + k_2)^2}{2m_b} - \epsilon_0}. \quad (\text{B1})$$

Now, for quadratic dispersions, the scattering amplitude f is related to the T -matrix as

$$f(k) = -i \frac{\mu}{k} T, \quad (\text{B2})$$

where $\mu = \frac{m}{2}$ is the reduced mass, and $k = \frac{k_1 - k_2}{2}$ is the reduced momentum. This leads to

$$f(k_1, k_2) = \frac{-ig^2}{\left(\frac{k_1}{m_a} - \frac{k_2}{m_a} \right) \left(\frac{k_1^2}{2m_a} + \frac{k_2^2}{2m_a} - \frac{(k_1 + k_2)^2}{2m_b} - \epsilon_0 \right) + ig^2}. \quad (\text{B3})$$

For ease of notation, we define

$$t_i \equiv \frac{1}{2m_i}, \quad i = a, b \quad (\text{B4})$$

such that the scattering amplitude equals

$$f = \frac{-ig^2}{2(k_1 t_a - k_2 t_a)(k_1^2 t_a + k_2^2 t_a - (k_1 + k_2)^2 t_b - \epsilon_0) + ig^2}. \quad (\text{B5})$$

We now linearise the spectrum about two Fermi momenta,

$$k_1 \approx k_{f1} + x_1, \quad k_2 \approx k_{f2} + x_2. \quad (\text{B6})$$

To linear order in x_i/k_{fi} , we thus find

$$f \approx \frac{-ig^2}{ig^2 + 2(v_1 - v_2)(x_1 v_1 + x_2 v_2 - u(x_1 + x_2) - \nu)}, \quad (\text{B7})$$

where we have defined the parameters

$$\begin{aligned}
v_1 &= \frac{\sqrt{t_a}}{d\sqrt{2}} \left((k_{f1} - k_{f2})^2 t_a - (k_{f1} + k_{f2})^2 t_b + 2k_{f1}^2 t_a - \epsilon_0 \right), \\
v_2 &= \frac{-\sqrt{t_a}}{d\sqrt{2}} \left((k_{f1} - k_{f2})^2 t_a - (k_{f1} + k_{f2})^2 t_b + 2k_{f2}^2 t_a - \epsilon_0 \right), \\
u &= \frac{2t_b}{d} \sqrt{\frac{t_a}{2}} (k_{f1}^2 - k_{f2}^2), \\
\nu &= \frac{(k_{f1} - k_{f2})\sqrt{t_a}}{d\sqrt{2}} \left((k_{f1}^2 + k_{f2}^2) t_a - (k_{f1} + k_{f2})^2 t_b - \epsilon_0 \right),
\end{aligned} \tag{B8}$$

and

$$d = \pm \sqrt{2t_a \left(k_{f1}^2 - k_{f1}k_{f2} + k_{f2}^2 \right) - t_b(k_{f1} + k_{f2})^2 - \epsilon_0}. \tag{B9}$$

Taking the positive root for d leads to $v_1 > v_2$, while the negative root results in $v_2 > v_1$.

In the continuum, we require that $m_b = 2m_a$, which pins the molecular velocity to that of the atoms, $u = (v_1 + v_2)/2$. However, on a lattice the effective mass of the molecule can be made independent of that of the atoms, in which case u can be varied (see App. C). Furthermore, in the case that $k_{f1} = k_{f2}$, we find that $v_2 = -v_1$ and $u = 0$. This corresponds to the case $v_1 > 0 > v_2$ with u lying in between, where unfortunately we are unable to find an analytic solution for the ground state densities (this is discussed in Sec. VII).

We note that to reach some of the regimes, for instance $u > v_1 > 0 > v_2$, we require a negative molecular mass, $m_b < 0$, which while not possible in the continuum, is allowed on a lattice. While the square root in the parameter d forces the original parameters $m_a, m_b, k_{f1}, k_{f2}, \nu$ to be chosen such that the velocities remain real, we will see that this linearisation procedure, when applied to the lattice two-channel model, allows us to access all the regimes

we study in the main text.

Appendix C: Linearisation of the lattice two-channel model

On a 1D lattice, the two-channel model is defined as

$$\begin{aligned}
H &= -t_a \sum_{\langle r, r' \rangle} c_{r, \sigma}^\dagger c_{r', \sigma} - t_b \sum_{\langle r, r' \rangle} b_r^\dagger b_{r'} + \epsilon_0 \sum_r b_r^\dagger b_r \\
&\quad + g \sum_r (b_r^\dagger c_{r, \uparrow} c_{r, \downarrow} + h.c.),
\end{aligned} \tag{C1}$$

where $c_{r, \sigma}, c_{r, \sigma}^\dagger$ are annihilation and creation operators for fermionic atoms with spin σ at the lattice site r , and b_r, b_r^\dagger are annihilation and creation operators for closed channel bosonic molecules. ϵ_0 is the bare detuning, g is the coupling, $t_a(t_b)$ are hopping matrix elements for atoms (molecules), and $\langle r, r' \rangle$ denotes nearest neighbour interactions. In the absence of interactions, the atoms and molecules are free particles with lattice dispersions,

$$\epsilon_k = -2t \cos(k), \tag{C2}$$

$$\epsilon_k^b = -2t_b \cos(k) + \epsilon_0, \tag{C3}$$

with the lattice constant, a , set to 1.

This model in three dimensions was studied in [47], using a mean-field analysis, where it was shown that when the band is more than half-filled and as the detuning is decreased (equivalently, attractive interactions are increased), the gas exhibits a non-monotonic crossover, from a paired BCS superfluid to a BEC of molecular holes, to the BCS, and to the BEC of molecules.

The scattering amplitude for this model can be calculated as described in App. A (where the momentum integration in the polarization operator Π now goes over the first Brillouin-zone, $k \in [-\pi, \pi]$),

$$f(k_1, k_2) = \frac{-ig^2}{ig^2 + 2t_a \left(\sin(k_1) - \sin(k_2) \right) \left(2t_b \cos(k_1 + k_2) - 2t_a (\cos(k_1) + \cos(k_2)) - \epsilon_0 \right)}. \tag{C4}$$

Similar to the continuum case, in the vicinity of two distinct Fermi momenta, $k_1 \approx k_{f1} + x_1$ and $k_2 \approx k_{f2} + x_2$,

this scattering amplitude reduces to that for the Q3WI (Eq. (A7)), where the velocities are now defined as

$$\begin{aligned}
v_1 &= -\frac{\sqrt{t_a}}{d} \left(2t_a \left(\cos(2k_{f1}) + \cos(k_{f1} - k_{f2}) \right) - \cos(k_{f1}) \left(2t_b \cos(k_{f1} + k_{f2}) - \epsilon_0 \right) \right), \\
v_2 &= \frac{\sqrt{t_a}}{d} \left(2t_a \left(\cos(2k_{f2}) + \cos(k_{f1} - k_{f2}) \right) - \cos(k_{f1}) \left(2t_b \cos(k_{f1} + k_{f2}) - \epsilon_0 \right) \right), \\
u &= 2t_b \frac{\sqrt{t_a}}{d} \sin(k_{f1} + k_{f2}) \left(\sin(k_{f1}) - \sin(k_{f2}) \right), \\
\nu &= -\frac{\sqrt{t_a}}{d} \left(2t_a \left(\cos(k_{f1}) + \cos(k_{f2}) \right) - 2t_b \cos(k_{f1} + k_{f2}) + \epsilon_0 \right) \left(\sin(k_{f1}) - \sin(k_{f2}) \right), \\
d &= \pm \sqrt{\left(\cos(k_{f1}) + \cos(k_{f2}) \right) \left(2t_b \cos(k_{f1} + k_{f2}) - \epsilon_0 \right) - 2t_a \left(\cos(2k_{f1}) + 2\cos(k_{f1} - k_{f2}) + \cos(2k_{f2}) \right)}. \quad (C5)
\end{aligned}$$

Taking the positive root for d leads to $v_1 > v_2$, while the negative root leads to the regime where $v_2 > v_1$. Thus, by varying the Fermi-points, k_{f1} and k_{f2} , the relative strengths of the atomic and molecular hoppings t_a, t_b , and the detuning ϵ_0 , we can explore all parameter regimes of the Q3WI model. Moreover, on the lattice we have more freedom as now t_a and t_b are independent, unlike in the continuum case.

Appendix D: Details for weakly interacting regime

In Sec. VI, we have discussed the general procedure for deriving the zero temperature ground state densities $\rho_i(k_i)$ and excitation spectra $\epsilon_i(k_i)$ in the weakly interacting regime for the cases when $u > v_1 > v_2$. Here, we present in detail the ground state densities, excitation spectra, and compressibilities for these cases. We reiterate that a host of other cases may be obtained from the ones discussed here; in particular, cases where $v_1 > v_2 > u$ can be obtained from the cases studied here by a combination of parity and fermion type exchange.

1. Case A: $u > v_1 > v_2$

For this case, the excitation spectra and ground state densities are found by taking the limit $T \rightarrow 0$ in Eq. (53) and Eq. (55) respectively. The special momenta $k_i^{(j)}$ ($j = a, b, c$) at which the derivatives $\epsilon'_i(k_i)$ may exhibit discontinuities are defined in Eq. (56). We note that case A1, which corresponds to $u > v_1 > v_2 > 0$, was analyzed in the main text and we will hence not repeat its discussion here.

a. Case A2i: $u > v_1 > 0 > v_2$ & $u < \frac{2v_1 v_2}{v_1 + v_2}$

For this case, we find that the parameter β , which satisfies $\text{sgn}(\beta) = \text{sgn}(\alpha)$, is

$$\begin{aligned}
\beta(D_1, D_2) &= 4\pi \left(\frac{D_2}{2u - v_1 - v_2} - \frac{D_1}{v_1 - v_2} \right) \\
&\quad - \frac{\nu}{(u - v_1)(u - v_2)}. \quad (D1)
\end{aligned}$$

The excitation spectra for this case are shown in the main text, Fig. 2. Depending on $\text{sgn}(\beta)$, the ground state densities and compressibilities are as follows:

For $\beta < 0$, the ground state densities are

$$\begin{aligned}
\rho_1(k_1) &= \begin{cases} \frac{1}{4\pi} \left(1 - \frac{u - v_1}{u - v_2} \right), & k_1 < k_1^{(a)}, \\ \frac{1}{2\pi}, & k_1^{(a)} < k_1 < k_1^f, \\ 0, & k_1 > k_1^f, \end{cases} \\
\rho_2(k_2) &= \begin{cases} 0, & k_2 < k_2^{(b)}, \\ \frac{1}{4\pi} \left(1 + \frac{u - v_2}{u - v_1} \right), & k_2 > k_2^{(b)}, \end{cases} \quad (D2)
\end{aligned}$$

where the Fermi momenta are

$$k_1^f = \frac{h_1}{v_1}, \quad k_2^f = k_2^{(b)}. \quad (D3)$$

These lead to the compressibility

$$\kappa^{-1} = 2\pi \begin{pmatrix} v_1 & v_1 \\ v_1 & \frac{3v_1 v_2 - 2uv_2 - v_1^2}{2u - v_1 - v_2} \end{pmatrix}. \quad (D4)$$

We note that the compressibilities are positive as required on physical grounds. In particular, $3v_1 v_2 - 2uv_2 - v_1^2 = 2v_1 v_2 - u(v_1 + v_2) + (u - v_1)(v_1 - v_2) > 0$ so that κ_{22}^{-1} is positive.

For $\beta = 0$, we find that

$$\begin{aligned} \rho_1(k_1) &= \begin{cases} \frac{1}{4\pi} \left(1 - \frac{u - v_1}{u - v_2}\right), & k_1 < k_1^f, \\ 0, & k_1 > k_1^f, \end{cases} \\ \rho_2(k_2) &= \begin{cases} 0, & k_2 < k_2^f, \\ \frac{1}{4\pi} \left(1 + \frac{u - v_2}{u - v_1}\right), & k_2 > k_2^f, \end{cases} \end{aligned} \quad (D5)$$

where in this case, both Fermi momenta are given by their values in the non-interacting case

$$k_1^f = \frac{h_1}{v_1}, \quad k_2^f = \frac{h_2}{v_2}. \quad (D6)$$

The compressibility associated with this case is

$$\kappa^{-1} = 4\pi \begin{pmatrix} v_1 \frac{u-v_2}{v_1-v_2} & 0 \\ 0 & -v_2 \frac{u-v_1}{2u-v_1-v_2} \end{pmatrix}. \quad (D7)$$

Finally, for $\beta > 0$ we find that the behavior again changes, with the momentum densities

$$\begin{aligned} \rho(k_1) &= \begin{cases} \frac{1}{4\pi} \left(1 - \frac{u - v_1}{u - v_2}\right), & k_1 < k_1^{(b)}, \\ 0, & k_1 > k_1^{(b)}, \end{cases} \\ \rho_2(k_2) &= \begin{cases} 0, & k_2 < k_2^f, \\ \frac{1}{2\pi}, & k_2^f < k_2 < k_2^{(a)}, \\ \frac{1}{4\pi} \left(1 + \frac{u - v_2}{u - v_1}\right), & k_2 > k_2^{(a)}, \end{cases} \end{aligned} \quad (D8)$$

such that the Fermi momenta in this case are

$$k_1^f = k_1^{(b)}, \quad k_2^f = \frac{h_2}{v_2}, \quad (D9)$$

leading to

$$\kappa^{-1} = 2\pi \begin{pmatrix} 2u - v_2 & v_2 \\ v_2 & -v_2 \end{pmatrix}. \quad (D10)$$

For this case, we see that for $\beta < 0$, the v_1 particles are non-interacting near their Fermi momentum while the v_2 particles are interacting throughout their Fermi sea. For $\beta > 0$ the roles are reversed since the v_1 fermions now interact throughout their Fermi sea while the v_2 particles become non-interacting in the vicinity of their Fermi momenta. The discontinuity in κ as β is changed captures precisely the change in the behavior of the fermions in the vicinity of their respective Fermi momenta.

b. Case A2ii: $u > v_1 > 0 > v_2$ & $u > \frac{2v_1v_2}{v_1+v_2}$

The parameter β in this case is simply related to the density D_2 of the v_2 fermions,

$$\beta(D_1, D_2) = D_2. \quad (D11)$$

Hence, in this case the regime where $\beta < 0$ is un-physical and we only consider the change in β as it acquires a non-vanishing value. The excitation spectra are shown in Fig. 3.

The case $\beta = 0$ corresponds to a vanishing density of v_2 particles and thus we expect that the v_1 particles should exhibit non-interacting behavior throughout the Fermi sea. This is indeed the case, since

$$\begin{aligned} \rho_1(k_1) &= \begin{cases} \frac{1}{2\pi}, & k_1 < k_1^f, \\ 0, & k_1 > k_1^f, \end{cases} \\ \rho_2(k_2) &= 0 \quad \forall k_2, \end{aligned} \quad (D12)$$

where the Fermi momentum $k_1^f = \frac{h_1}{v_1}$ equals its value in the non-interacting case. Moreover, the compressibility κ_{11} also matches that for non-interacting chiral fermions

$$\kappa^{-1} = 2\pi \begin{pmatrix} v_1 & 0 \\ 0 & 0 \end{pmatrix}. \quad (D13)$$

Once we have a finite density of v_2 particles, $\beta = D_2 > 0$, and the ground state densities become

$$\begin{aligned} \rho_1(k_1) &= \begin{cases} \frac{1}{2\pi}, & k_1 < k_1^{(a)}, \\ \frac{1}{4\pi} \left(1 - \frac{u - v_1}{u - v_2}\right), & k_1^{(a)} < k_1 < k_1^{(b)}, \\ 0, & k_1 > k_1^{(b)}, \end{cases} \\ \rho_2(k_2) &= \begin{cases} 0, & k_2 < k_2^{f,1}, \\ \frac{1}{2\pi}, & k_2^{f,1} < k_2 < k_2^{(a)}, \\ \frac{1}{4\pi} \left(1 + \frac{u - v_2}{u - v_1}\right), & k_2^{(a)} < k_2 < k_2^{(b)}, \\ 0, & k_2 > k_2^{(b)}. \end{cases} \end{aligned} \quad (D14)$$

Here, the fermions with velocity v_1 have a single Fermi momentum while the spectrum for the other species crosses zero energy twice, resulting in two Fermi momenta for that species,

$$k_1^f = k_1^{(b)}, \quad k_2^{f,1} = \frac{h_2}{v_2}, \quad k_2^{f,2} = k_2^{(b)}. \quad (D15)$$

The associated compressibilities in this case are

$$\kappa^{-1} = 2\pi \begin{pmatrix} v_1 & -v_2 \frac{u-v_1}{u-v_2} \\ -v_2 \frac{u-v_1}{u-v_2} & -v_2 \frac{u^2-v_1v_2}{(u-v_2)^2} \end{pmatrix}. \quad (D16)$$

Here, the v_1 particles interact near the Fermi sea while the v_2 particles develop two Fermi momenta as a consequence of their spectrum $\epsilon_2(k_2)$ becoming non-chiral.

c. Case A3: $u > 0 > v_1 > v_2$

For this case, we find that

$$\beta(D_1, D_2) = \frac{\nu(2u - v_1 - v_2)}{(u - v_1)(u - v_2)} - 4\pi(D_1 + D_2). \quad (D17)$$

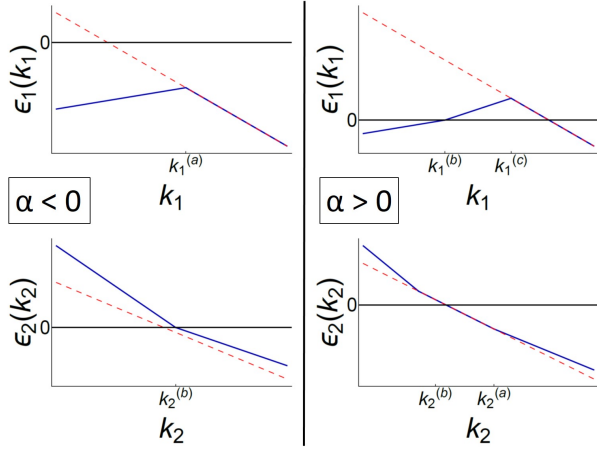


FIG. 7. Excitation spectra for case A3, with $u = 8, v_1 = -3, v_2 = -6, h_1 = 1, h_2 = 2$. The plots on the left are for $\alpha < 0$ ($\nu = -10$) in which case the v_1 fermions do not develop a Fermi momentum. The right-hand panel corresponds to $\alpha > 0$ ($\nu = 30$) where the v_1 particles develop two distinct Fermi momenta and where the v_2 particles are interacting deep into the Fermi sea. The red dashed lines are the excitation spectra for a non-interacting system ($g = 0$).

Here, we find that $\beta < 0$ implies the lack of any Fermi momentum for the v_1 particles i.e., $\epsilon_\rho(k) < 0 \forall k$ as depicted in the left panel of Fig. 7. Since there is no Fermi momentum, we cannot find a relation between the particle densities D_i and the chemical potentials h_i , such that the compressibility is an ill-defined quantity in this case.

However, for $\beta = 0$ the v_1 particles develop a Fermi momentum and we find that

$$\rho_1(k_1) = \begin{cases} \frac{1}{4\pi} \left(1 - \frac{u - v_1}{u - v_2} \right), & k_1 < k_1^f, \\ \frac{1}{2\pi}, & k_1 > k_1^f, \end{cases}$$

$$\rho_2(k_2) = \begin{cases} 0, & k_2 < k_2^f, \\ \frac{1}{4\pi} \left(1 + \frac{u - v_2}{u - v_1} \right), & k_2 > k_2^f, \end{cases} \quad (\text{D18})$$

where the Fermi momenta take on their non-interacting values,

$$k_1^f = \frac{h_1}{v_1}, \quad k_2^f = \frac{h_2}{v_2}, \quad (\text{D19})$$

from which we find

$$\kappa^{-1} = -\frac{4\pi}{2u - v_1 - v_2} \begin{pmatrix} v_1(u - v_2) & 0 \\ 0 & v_2(u - v_1) \end{pmatrix}. \quad (\text{D20})$$

For $\beta > 0$, we find that the behavior changes and, similar to the previous case Sec. D1b, we find that the v_1 fermions no longer have a fixed chirality due to the weak interactions. Furthermore, the v_2 particles remain interacting deep within the Fermi sea and it is only in

the vicinity of their Fermi momentum that they do not interact. This is reflected in the ground state densities,

$$\rho_1(k_1) = \begin{cases} \frac{1}{4\pi} \left(1 - \frac{u - v_1}{u - v_2} \right), & k_1 < k_1^{(b)}, \\ 0, & k_1^{(b)} < k_1 < k_1^{f,1}, \\ \frac{1}{2\pi}, & k_1 > k_1^{f,1}, \end{cases}$$

$$\rho_2(k_2) = \begin{cases} 0, & k < k_2^f, \\ \frac{1}{2\pi}, & k_2^f < k_2 < k_2^{(a)}, \\ \frac{1}{4\pi} \left(1 + \frac{u - v_2}{u - v_1} \right), & k_2 > k_2^{(a)}. \end{cases} \quad (\text{D21})$$

Here the first species of fermions, with velocity v_1 , develop two Fermi momenta since their spectrum crosses zero energy twice, while the second species of fermions have a Fermi momentum that takes on its non-interacting value,

$$k_1^{f,1} = \frac{h_1}{v_1}, \quad k_1^{f,2} = k_2^{(b)}, \quad k_2^f = \frac{h_2}{v_2}. \quad (\text{D22})$$

From these ground state densities, we derive

$$\kappa^{-1} = -\frac{2\pi}{2u - v_1 - v_2} \begin{pmatrix} v_1(2u - v_2) & v_1 v_2 \\ v_1 v_2 & v_2(2u - v_1) \end{pmatrix}. \quad (\text{D23})$$

As in all previous cases, the discontinuity in the compressibilities κ indicates the phase transition that occurs in the Q3WI model as a function of the particle densities D_i and the detuning ν . In addition to the v_1 particles being non-chiral for $\beta > 0$, this case exhibits the peculiar behavior that when $\beta < 0$, the v_1 fermions are unable to develop a Fermi momentum, with κ ill-defined in this regime.

d. Case A4: $0 > u > v_1 > v_2$

This is the final region of parameter space which appears in case A. Here, we find that

$$\beta(D_1, D_2) = \nu - 2\pi D_1(u - v_1) - 2\pi D_2(u - v_2). \quad (\text{D24})$$

For $\beta < 0$, we find that both species of fermions remain non-interacting deep within the Fermi sea but interact in the vicinity of their Fermi momenta, as shown in Fig. 8

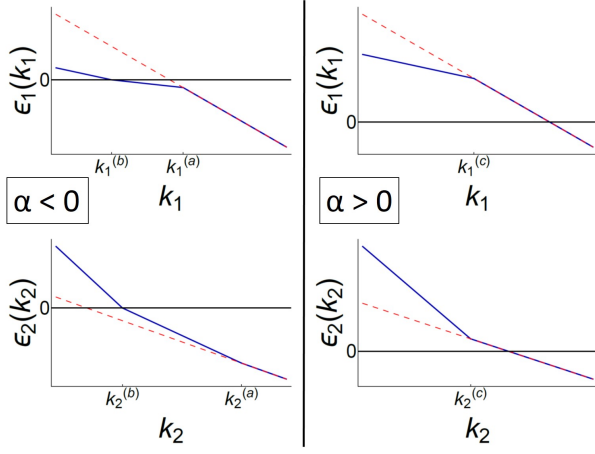


FIG. 8. Excitation spectra for case A4, with $u = -2, v_1 = -4, v_2 = -10, h_1 = 1, h_2 = 2$. The plots on the left are for $\nu = -10$, so for $\alpha < 0$, while the ones on the right are for $\nu = 10$, so for $\alpha > 0$. The red dashed lines are the excitation spectra for a non-interacting system.

and reflected in the ground state densities

$$\rho_1(k_1) = \begin{cases} 0, & k_1 < k_1^{(b)}, \\ \frac{1}{4\pi} \left(1 - \frac{u - v_1}{u - v_2} \right), & k_1^{(b)} < k_1 < k_1^{(a)}, \\ \frac{1}{2\pi}, & k_1 > k_1^{(a)}, \end{cases}$$

$$\rho_2(k_2) = \begin{cases} 0, & k_2 < k_2^{(b)}, \\ \frac{1}{4\pi} \left(1 + \frac{u - v_2}{u - v_1} \right), & k_2^{(b)} < k_2 < k_2^{(a)}, \\ \frac{1}{2\pi}, & k_2 > k_2^{(a)}, \end{cases} \quad (\text{D25})$$

with the Fermi momenta

$$k_1^f = k_1^{(b)}, \quad k_2^f = k_2^{(b)}, \quad (\text{D26})$$

and associated compressibilities,

$$\kappa^{-1} = \frac{-2\pi}{2u - v_1 - v_2} \begin{pmatrix} u^2 - v_1 v_2 & (u - v_1)(u - v_2) \\ (u - v_1)(u - v_2) & u^2 - v_1 v_2 \end{pmatrix}. \quad (\text{D27})$$

The behavior simplifies for $\beta \geq 0$ where we find that both species of fermions remain completely non-interacting throughout the Fermi sea,

$$\rho_1(k_1) = \begin{cases} 0, & k_1 < k_1^f, \\ \frac{1}{2\pi}, & k_1 > k_1^f, \end{cases}$$

$$\rho_2(k_2) = \begin{cases} 0, & k_2 < k_2^f, \\ \frac{1}{2\pi}, & k_2 > k_2^f, \end{cases} \quad (\text{D28})$$

with Fermi momentum $k_i^f = h_i/v_i$ and compressibility

$$\kappa^{-1} = -2\pi \begin{pmatrix} v_1 & 0 \\ 0 & v_2 \end{pmatrix}, \quad (\text{D29})$$

also corresponding to that of non-interacting chiral fermions. We note that qualitatively this case is similar in nature to case A1, which is discussed in the main text.

Thus, in each of the preceding cases, we have demonstrated that the compressibilities κ display a discontinuity as a function of D_1, D_2, ν since the ground state densities $\rho_i(k_i)$ are discontinuous. We further note that in each case κ_{ii} ($i = 1, 2$) are positive, as required on physical grounds. We see that $\det(\kappa) > 0$ in each case as well.

Appendix E: Solution to Integral Equations

Here, we discuss the procedure for finding a solution to an integral equation of the form encountered in the main text, Eq. (96). To do this, we consider a more general integral equation of the form

$$\int_a^b d\mu \frac{\phi(\mu)}{(\mu - \lambda)^2} = f(\lambda), \quad \lambda \in (a, b). \quad (\text{E1})$$

Then, we define

$$\mu = \frac{b-a}{2}x + \frac{b+a}{2}, \quad \lambda = \frac{b-a}{2}y + \frac{b+a}{2}, \quad (\text{E2})$$

such that $x, y \in [-1, 1]$ and $\mu - \lambda = \frac{b-a}{2}(x - y)$. This leads to

$$\int_{-1}^1 dx \frac{\phi\left(\frac{b-a}{2}x + \frac{b+a}{2}\right)}{(x - y)^2} = \frac{b-a}{2} f\left(\frac{b-a}{2}y + \frac{b+a}{2}\right), \quad (\text{E3})$$

or, equivalently

$$\int_{-1}^1 dx \frac{A(x)}{(x - y)^2} = B(y), \quad y \in [-1, 1], \quad (\text{E4})$$

where $A(x) = \phi(\mu)$ and $B(y) = \frac{b-a}{2}f(\lambda)$.

From the general theory of hyper-singular equations, (see, e.g. Refs. [48, 49]), the solution to the above equation is known to be

$$A(y) = \int_{-1}^y \frac{d\tau}{\sqrt{1-\tau^2}} \int_{-1}^1 dx \frac{\sqrt{1-x^2} B(x)}{\tau - x \pi^2},$$

$$= \int_{-1}^1 dx \frac{B(x)}{\pi^2} \log \left[\frac{\sqrt{(1-x)(1+y)} - \sqrt{(1+x)(1-y)}}{\sqrt{(1-x)(1+y)} + \sqrt{(1+x)(1-y)}} \right]. \quad (\text{E5})$$

For instance, for $B(y) = C$, a constant, we find

$$A(x) = -\frac{C}{\pi} \sqrt{1-x^2}, \quad x \in [-1, 1], \quad (\text{E6})$$

while for $B(y) = Cy$, we find

$$A(x) = -\frac{C}{2\pi} x \sqrt{1-x^2}, \quad x \in [-1, 1]. \quad (\text{E7})$$

Appendix F: Compressibilities in the Quasi-Condensate regime

In this Appendix, we discuss in detail the calculation establishing the ground state compressibility (102) for the quasi-condensate regime (see Sec. VII).

Specifically, let us consider the case where $v_1 > u > v_2 > 0$ and where the parameter $\alpha < 0$. The behavior of the fermions in this regime is depicted in Fig. 4 and the ground state densities to leading order are given by Eqs. (94), (97), and (98). For ease of notation, we denote the Fermi momenta throughout this section as

$$K_i \equiv k_i^f. \quad (\text{F1})$$

In what follows, we will require knowledge of the matrix of derivatives

$$M_{ij} = \frac{\partial K_i}{\partial D_j} = (V^{-1})_{ij}, \quad (\text{F2})$$

where the matrix V is defined as

$$V_{ij} = \frac{\partial D_i}{\partial K_j}. \quad (\text{F3})$$

From Fig. 4 and the expressions for ρ_i , we see that the density of the first fermionic species D_1 depends non-trivially on the Fermi momentum of both species of fermions since the parameter $k_1^{(i)}$ is a function of K_2 (see Eq. (89)). However, the density of the other species D_2 depends only on its own Fermi momentum K_2 , so that

$$\frac{\partial D_2}{\partial K_1} = 0. \quad (\text{F4})$$

We also note that while the particle densities and total energy diverge in the limit $g \rightarrow 0$, their derivatives may remain finite. For instance, the only dependence of D_1 on K_1 comes from the range of momenta over which ρ_1 takes its non-interacting value, from which we can show that

$$\frac{\partial D_1}{\partial K_1} = \frac{1}{2\pi} + O(g^2). \quad (\text{F5})$$

Similarly,

$$\frac{\partial^2 \mathcal{E}}{\partial K_1^2} = \frac{v_1}{2\pi} + O(g^2). \quad (\text{F6})$$

We hence find that the expressions for the compressibilities simplify considerably. For the inverse compressibility of the first species of fermions we find that

$$[\kappa]_{11}^{-1} = \left(\frac{\partial D_1}{\partial K_1} \right)^{-2} \frac{\partial^2 \mathcal{E}}{\partial K_1^2} = 2\pi v_1 + O(g^2), \quad (\text{F7})$$

which reflects the fact that ρ_1 takes its non-interacting value of $1/(2\pi)$ in the vicinity of K_1 .

Next, we consider the mixed term

$$[\kappa]_{12}^{-1} = -2\pi v_1 \left(\frac{\partial D_1}{\partial K_2} \right) \left(\frac{\partial D_2}{\partial K_2} \right)^{-1} = [\kappa]_{21}^{-1}. \quad (\text{F8})$$

Crucially, we see from Fig. 4 that the dependence of D_1 (D_2) on K_2 comes through the region where ρ_1 (ρ_2) takes its interacting value and since we know that our analytic solution for ρ_1 breaks down in the vicinity of K_2 , care must be taken when evaluating a term such as $\partial D_1/\partial K_2$. In particular, we must account for the possibility that corrections to our analytic solution alter the leading order solution for κ^{-1} . This issue does not arise for our solutions in the non-interacting regions since any corrections to the $1/(2\pi)$ density in those regions vanish as $g \rightarrow 0$. Since our analytic solutions within the interacting regions $\sim 1/g^2$ however, corrections to those may still diverge in the limit $g \rightarrow 0$ and hence must be treated more carefully.

In order to take into account the effect of corrections to our analytic solution within the interacting regions, let us consider

$$\frac{\partial D_1}{\partial K_2} = \frac{\partial}{\partial K_2} \left[\int_{-\Lambda}^{k_1^{(i)}} dk_1 \tilde{\rho}_1(k_1) + \frac{1}{2\pi} \int_{k_1^{(i)}}^{K_1} dk_1 \right], \quad (\text{F9})$$

where $k_1^{(i)}$ depends on K_2 and where

$$\tilde{\rho}_1 = \rho_1 + \delta\rho_1, \quad (\text{F10})$$

with $\delta\rho_1$ representing corrections to our leading order solution ρ_1 in the interacting region, given by Eq. (97). We can further simplify the above expression to find

$$\frac{\partial D_1}{\partial K_2} = \left(\tilde{\rho}_1(k_1^{(i)}) - \frac{1}{2\pi} \right) \frac{dk_1^{(i)}}{\partial K_2} + \int_{-\Lambda}^{k_1^{(i)}} dk_1 \frac{\partial}{\partial K_2} \tilde{\rho}_1(k_1). \quad (\text{F11})$$

Now, while our analytical solution Eq. (97) for ρ_1 vanishes at $k_1^{(i)}$, we know that this is merely an artefact of the small g approximation and that the real solution should connect smoothly with $1/(2\pi)$. Thus, we expect that

$$\frac{\partial D_1}{\partial K_2} = \int_{-\Lambda}^{k_1^{(i)}} dk_1 \frac{\partial}{\partial K_2} \tilde{\rho}_1(k_1), \quad (\text{F12})$$

where the dependence of $\tilde{\rho}_1$ on K_2 is implicit.

A similar analysis demonstrates that

$$\frac{\partial D_2}{\partial K_2} = \tilde{\rho}_2(K_2) + \int_{-\Lambda_0}^{K_2} dk_2 \frac{\partial}{\partial K_2} \tilde{\rho}_2(k_2), \quad (\text{F13})$$

with

$$\tilde{\rho}_2 = \rho_2 + \delta\rho_2, \quad (\text{F14})$$

where $\delta\rho_2$ represents corrections to our leading order solution ρ_2 in the interacting region, given by Eq. (98). Again, we note that our leading order solution vanishes

exactly at K_2 i.e., $\rho_2(K_2) = 0$, but we expect that the true solution will remain finite at the end point, in analogy with the Lieb-Liniger gas.

Importantly, we note that since our leading order analytic solutions $\sim 1/g^2$, any corrections to these must be less singular i.e., $\delta\rho_i \sim 1/g^\alpha$ with $\alpha < 2$. Consequently, any corrections to the derivatives $\partial D_i/\partial K_2$ must also be less singular and we thus find that the ratio

$$\left(\frac{\partial D_1}{\partial K_2}\right) \left(\frac{\partial D_2}{\partial K_2}\right)^{-1} = 1 + O(g) \quad (\text{F15})$$

in the limit $g \rightarrow 0$, since our leading order solutions for the ground state densities satisfy

$$\int_{-\Lambda}^{k_1^{(i)}} dk_1 \frac{\partial}{\partial K_2} \rho_1(k_1) = \int_{-\Lambda_0}^{K_2} dk_2 \frac{\partial}{\partial K_2} \rho_2(k_2), \quad (\text{F16})$$

and because all contributions from the corrections $\delta\rho_i$ vanish as $g \rightarrow 0$. We have hence established that it is sufficient to consider our analytic expressions for the ground state densities, derived in the main text, in order to find the leading order compressibilities. Following the above discussion, we find that

$$[\kappa]_{12}^{-1} = -2\pi v_1 + O(g) = [\kappa]_{21}^{-1}. \quad (\text{F17})$$

Similarly, we can establish that

$$[\kappa]_{22}^{-1} = 2\pi v_1 + O(g). \quad (\text{F18})$$

To demonstrate that the inverse compressibility matrix κ^{-1} is invertible at next-to-leading order, we note that

$$[\kappa]_{22}^{-1} = \frac{\partial^2 \mathcal{E}}{\partial D_2^2} = \frac{1}{2\pi v_1} [\kappa]_{12}^{-2} + \Gamma, \quad (\text{F19})$$

where

$$\begin{aligned} \Gamma = & \left(\frac{\partial D_2}{\partial K_2}\right)^{-2} \frac{\partial^2 \mathcal{E}}{\partial K_2^2} \\ & + \left(\frac{\partial D_2}{\partial K_2}\right)^{-1} \frac{\partial \mathcal{E}}{\partial K_2} \frac{\partial}{\partial K_2} \left[\left(\frac{\partial D_2}{\partial K_2}\right)^{-1} \left(1 - 2\pi \frac{\partial D_1}{\partial K_2}\right) \right]. \end{aligned} \quad (\text{F20})$$

Following the above discussion, we have seen that we can write

$$[\kappa]_{12}^{-1} = -2\pi v_1(1 + \epsilon_1) \quad (\text{F21})$$

where $\epsilon_1 \rightarrow 0$ as $g \rightarrow 0$. Similarly, we can evaluate the behavior of Γ while taking into account corrections to the leading order behavior of ρ_i and we find that

$$\Gamma = 2\pi v_1 \epsilon_2, \quad (\text{F22})$$

where $\epsilon_2 \rightarrow 0$ as $g \rightarrow 0$ i.e., there is no finite contribution to Γ from the leading order solution in the limit of small g . We can now write

$$[\kappa]_{22}^{-1} = 2\pi v_1[(1 + \epsilon_1)^2 + \epsilon_2] \approx 2\pi v_1(1 + 2\epsilon_1 + \epsilon_2) \quad (\text{F23})$$

as $g \rightarrow 0$. Thus, the inverse compressibility matrix, accounting for the leading order corrections is

$$\kappa^{-1} = \begin{pmatrix} 2\pi v_1 & -2\pi v_1(1 + \epsilon_1) \\ -2\pi v_1(1 + \epsilon_1) & 2\pi v_1(1 + 2\epsilon_1 + \epsilon_2) \end{pmatrix}, \quad (\text{F24})$$

with a determinant given by

$$\det(\kappa^{-1}) = (2\pi v_1)^2 \epsilon_2 \quad (\text{F25})$$

to leading order in g . Hence, we see that that non-invertible nature of κ^{-1} is a consequence of the small g approximation and that it is necessary to establish corrections to the analytical solutions developed in this paper in order to find the compressibility matrix κ . While we have discussed the specific case when $\alpha < 0$ here, the case when $\alpha > 0$ can be analyzed similarly.

-
- [1] C. A. Regal, C. Ticknor, J. L. Bohn, and D. S. Jin, *Nature* **424**, 47 (2003).
 - [2] S. Inouye, J. Goldwin, M. L. Olsen, C. Ticknor, J. L. Bohn, and D. S. Jin, *Phys. Rev. Lett.* **93**, 183201 (2004).
 - [3] C. A. Stan, M. W. Zwierlein, C. H. Schunck, S. M. F. Raupach, and W. Ketterle, *Phys. Rev. Lett.* **93**, 143001 (2004).
 - [4] K. Günter, T. Stöferle, H. Moritz, M. Köhl, and T. Esslinger, *Phys. Rev. Lett.* **96**, 180402 (2006).
 - [5] T. Best, S. Will, U. Schneider, L. Hackermüller, D. van Oosten, I. Bloch, and D.-S. Lühmann, *Phys. Rev. Lett.* **102**, 030408 (2009).
 - [6] B. Paredes, A. Widera, V. Murg, O. Mandel, S. Fölling, I. Cirac, G. V. Shlyapnikov, T. W. Hänsch, and I. Bloch, *Nature* **429**, 277 (2004).
 - [7] T. Kinoshita, T. Wenger, and D. S. Weiss, *Science* **305**, 1125 (2004).
 - [8] E. Haller, M. Gustavsson, M. J. Mark, J. G. Danzl, R. Hart, G. Pupillo, and H.-C. Nägerl, *Science* **325**, 1224 (2009).
 - [9] K. Günter, T. Stöferle, H. Moritz, M. Köhl, and T. Esslinger, *Phys. Rev. Lett.* **95**, 230401 (2005).
 - [10] H. Moritz, T. Stöferle, K. Günter, M. Köhl, and T. Esslinger, *Phys. Rev. Lett.* **94**, 210401 (2005).
 - [11] Y.-A. Liao, A. S. C. Rittner, T. Paprotta, W. Li, G. B. Partridge, R. G. Hulet, S. K. Baur, and E. J. Mueller, *Nature* **467**, 567 (2010).
 - [12] K. K. Das, *Phys. Rev. Lett.* **90**, 170403 (2003).
 - [13] X. Yin, X.-W. Guan, Y. Zhang, and S. Chen, *Phys. Rev. A* **85**, 013608 (2012).
 - [14] M. T. Batchelor, M. Bortz, X. W. Guan, and N. Oelkers, *Phys. Rev. A* **72**, 061603 (2005).
 - [15] X.-W. Guan, M. T. Batchelor, and J.-Y. Lee, *Phys. Rev. A* **78**, 023621 (2008).
 - [16] A. Imambekov and E. Demler, *Phys. Rev. A* **73**, 021602 (2006); *Ann. Phys.* **321**, 2390 (2006).
 - [17] L. Mathey, D.-W. Wang, W. Hofstetter, M. D. Lukin, and E. Demler, *Phys. Rev. Lett.* **93**, 120404 (2004).
 - [18] M. A. Cazalilla and A. F. Ho, *Phys. Rev. Lett.* **91**, 150403 (2003).
 - [19] L. Viverit and S. Giorgini, *Phys. Rev. A* **66**, 063604 (2002).
 - [20] A. Imambekov, A. A. Lukyanov, L. I. Glazman, and V. Gritsev, *Phys. Rev. Lett.* **104**, 040402 (2010).
 - [21] R. Friedberg and T. D. Lee, *Phys. Lett. A* **138**, 423 (1989a); *Phys. Rev. B* **40**, 6745 (1989).
 - [22] M. Holland, S. J. J. M. F. Kokkelmans, M. L. Chiofalo, and R. Walser, *Phys. Rev. Lett.* **87**, 120406 (2001).
 - [23] E. Timmermans, K. Furuya, P. W. Milonni, and A. K. Kerman, *Phys. Lett. A* **285**, 228 (2001).
 - [24] V. Gurarie and L. Radzihovsky, *Ann. Phys.* **322**, 2 (2007).
 - [25] A. Recati, J. N. Fuchs, and W. Zwerger, *Phys. Rev. A* **71**, 033630 (2005).
 - [26] H. A. Bethe, *Z. Phys.* **71**, 205 (1931).
 - [27] M. Gaudin, *Phys. Lett. A* **24**, 55 (1967).
 - [28] M. Gaudin, Ph.D. thesis, University of Paris (1967).
 - [29] C. N. Yang, *Phys. Rev. Lett.* **19**, 1312 (1967).
 - [30] J. N. Fuchs, A. Recati, and W. Zwerger, *Phys. Rev. Lett.* **93**, 090408 (2004).
 - [31] I. V. Tokatly, *Phys. Rev. Lett.* **93**, 090405 (2004).
 - [32] V. Gurarie, *Phys. Rev. A* **73**, 033612 (2006).
 - [33] D. E. Sheehy and L. Radzihovsky, *Phys. Rev. Lett.* **95**, 130401 (2005).
 - [34] E. Orignac and R. Citro, *Phys. Rev. A* **73**, 063611 (2006).
 - [35] K. Ohkuma and M. Wadati, *J. Phys. Soc. Jpn.* **53**, 2899 (1984).
 - [36] M. Wadati and K. Ohkuma, *J. Phys. Soc. Jpn.* **53**, 1229 (1984).
 - [37] K. Ohkuma, *J. Phys. Soc. Jpn.* **54**, 2817 (1985).
 - [38] E. H. Lieb and W. Liniger, *Phys. Rev.* **130**, 1605 (1963).
 - [39] E. H. Lieb, *Phys. Rev.* **130**, 1616 (1963).
 - [40] T. Cheon and T. Shigehara, *Phys. Rev. Lett.* **82**, 2536 (1999).
 - [41] V. I. Yukalov and M. D. Girardeau, *Laser Phys. Lett.* **2**, 375 (2005).
 - [42] M. Khodas, M. Pustilnik, A. Kamenev, and L. I. Glazman, *Phys. Rev. Lett.* **99**, 110405 (2007).
 - [43] V. E. Korepin, N. M. Bogoliubov, and A. G. Izergin, *Quantum Inverse Scattering Method and Correlation Functions*, Cambridge Monographs on Mathematical Physics (Cambridge University Press, 1993).
 - [44] R. Beals, D. Sattinger, and E. Williams, *J. Math. Phys.* **39**, 1 (1998).
 - [45] C. N. Yang and C. P. Yang, *J. Math. Phys.* **10**, 1115 (1969).
 - [46] M. Takahashi, *Thermodynamics of One-Dimensional Solvable Models* (Cambridge University Press, 1999).
 - [47] Z. Shen, L. Radzihovsky, and V. Gurarie, *Phys. Rev. Lett.* **109**, 245302 (2012).
 - [48] N. I. Muskhelishvili, *Singular integral equations* (Dover Publications, 2008).
 - [49] I. K. Lifanov, L. N. Poltavskii, and G. M. Vainikko, *Hypersingular Integral Equations and their Applications*, edited by A. D. Polyanon (Chapman & Hall/CRC, 2004).